Inorganic Chemistry

pubs.acs.org/IC

Article

Manganese(I) Complex with Monodentate Arylisocyanide Ligands Shows Photodissociation Instead of Luminescence

Sascha Ossinger, Alessandro Prescimone, Daniel Häussinger, and Oliver S. Wenger*

Cite This: *Inorg. Chem.* 2022, 61, 10533−10547

Read Online

ACCESS | Metrics & More | Article Recommendations | Supporting Information

ABSTRACT: Recently reported manganese(I) complexes with chelating arylisocyanide ligands exhibit luminescent metal-to-ligand charge-transfer (MLCT) excited states, similar to ruthenium(II) polypyridine complexes with the same d^6 valence electron configuration used for many different applications in photophysics and photochemistry. However, chelating arylisocyanide ligands require substantial synthetic effort, and therefore it seemed attractive to explore the possibility of using more readily accessible monodentate arylisocyanides instead. Here, we synthesized the new Mn(I) complex $[Mn(CNdippPh^{OMe2})_6]PF_6$ with the known ligand $CNdippPh^{OMe2}$ = 4-(3,5-dimethoxyphenyl)-2,6-diisopropylphenylisocyanide. This complex was investigated by NMR spectroscopy, single-crystal structure analysis, high-resolution electrospray ionization mass spectrometry (HR-ESI-MS) measurements, IR spectroscopy supported by density functional theory (DFT) calculations, cyclic voltammetry, and time-resolved as well as steady-state UV−vis absorption spectroscopy. The key finding is that the new Mn(I) complex is nonluminescent and instead undergoes arylisocyanide ligand loss during continuous visible laser irradiation into ligand-centered and charge-transfer absorption bands, presumably owed to the population of dissociative d−d excited states. Thus, it seems that chelating bi- or tridentate binding motifs are essential for obtaining emissive MLCT excited states in manganese(I) arylisocyanides. Our work contributes to understanding the basic properties of photoactive first-row transition metal complexes and could help advance the search for alternatives to precious metal-based luminophores, photocatalysts, and sensors.

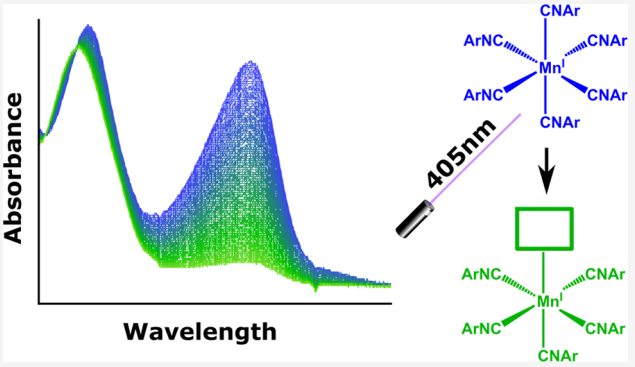

1. INTRODUCTION

Metal-to-ligand charge-transfer (MLCT) excited states play a key role in many coordination complexes and organometallic compounds because they enable a range of different applications in photophysics and photochemistry. Precious and rare elements such as ruthenium(II),[1−5] osmium(II),[6−10] rhenium(I),[11−19] or iridium(III)[16,20−26] in polypyridine or cyclometalating coordination environments often feature a long-lived MLCT excited state,[27,28] whereas among first-row d^6 transition metal elements, this is yet a very rare occurrence. Iron(II) is by far most investigated in this regard,[29−45] yet only a handful of iron(II) complexes with MLCT lifetimes in the nanosecond time regime are known.[29,30,42] Building on early reports of hexakis(arylisocyanide) manganese(I) complexes with a focus on UV−vis absorption and electrochemical properties,[46−53] we recently discovered that manganese(I) complexes with chelating bi- and tridentate ligands have luminescent and photoredox active MLCT states.[54] Until now, the synthesis of these chelates has remained laborious,[55] and therefore it seemed attractive to explore the possibility of using more directly accessible monodentate arylisocyanides for manganese(I) complexes with luminescent MLCT states. Recently, there has been increased interest in first-row transition metal elements, partly because they are cheaper and more abundant than the traditionally used metals from the platinum group,[56] and because they seem to offer ample opportunities for groundbreaking discoveries.[57−60] Advances in ligand design, photophysical techniques, and theoretical understanding[61] have made an unexpectedly broad range of transition metals in different oxidation states useable for photophysical or photochemical applications. In particular, luminescent first-row transition metal complexes with V,[62−65] Cr,[66−74] Mn,[54,75−77] Fe,[29,35,43,78−80] Co,[72,81−84] Ni,[85−88] and Cu[89−98] with different types of electronically excited states featuring promising photoreactivity and photoluminescence behavior have been discovered recently.[57,58,60,99,100]

As early as 1977, Mann, Gray, and Hammond reported on tungsten(0) arylisocyanide complexes that showed MLCT

Received: April 27, 2022
Published: June 29, 2022

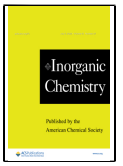

luminescence in solution at room temperature.[101] More recently, the GRAY group revisited this topic and discovered a whole range of $[W(CNAryl)_6]$,[102−107] complexes with outstanding photoluminescence properties and very strong photoreducing behavior with applications in catalysis. In addition to diisopropyl substituents at the *ortho*-position to the ligating isocyanide functional group, the attachment of further phenyl rings at the *para*-position proved valuable to enhance the chemical stability and the photophysical properties of this compound class, for example in $[W(CNdippPh^{OMe2})_6]$ ($CNdippPh^{OMe2}$ = 4-(3,5-dimethoxyphenyl)-2,6-diisopropylphenylisocyanide).[103] This specific tungsten(0) complex featured a high photoluminescence quantum yield (0.42) paired with a long MLCT lifetime (1.65 μs in toluene at room temperature), hence our interest in this particular ligand for manganese(I).[103]

In the recent past, other oxidation states of manganese received attention in the context of photoluminescence; for instance, many manganese(II) compounds are known to emit in the solid state.[75] Furthermore, a bis-(tris(carbene)borate) manganese(IV) complex featured dual luminescence from LMCT (ligand-to-metal charge-transfer) and metal-centered (MC) excited states.[77] At present, the photophysics of manganese(I) isocyanide complexes seems underexplored yet, particularly in comparison to isoelectronic iron(II) polypyridines.[29,30,32−34,38−45,80,108−118] By contrast, tricarbonyl complexes of manganese(I) represent a fairly well-investigated class of compounds, which can undergo phototriggered loss of CO ligands. Consequently, they belong to the so-called photoCORM family of compounds, i. e., photoactive carbon monoxide-releasing molecules, that are interesting for the light-controlled delivery of CO for therapeutic purposes.[76,119−132]

Here, we report on the new complex $[Mn(CNdippPh^{OMe2})_6]PF_6$ ($CNdippPh^{OMe2}$ = 4-(3,5-dimethoxyphenyl)-2,6-diisopropylphenylisocyanide), including detailed structural, vibrational, electrochemical, and photophysical studies.

2. EXPERIMENTAL SECTION

2.1. Physical Measurements. NMR spectra were recorded in deuterated solvents on a Bruker Avance III NMR spectrometer operating at a ^1H frequency of 600 or 400 MHz, a ^{13}C frequency of 151 or 100 MHz, ^{31}P and ^{19}F frequencies of 565 and 243 MHz, respectively, at 298 K. All chemical shifts are reported in δ values in ppm relative to tetramethylsilane (TMS), referred to protons of the residual nondeuterated solvent used or its carbon atoms, respectively (^1H: $\delta(CD_2Cl_2)$ = 5.32 ppm, $\delta(CDCl_3)$ = 7.26 ppm), the solvent signal (^{13}C: $\delta(CD_2Cl_2)$ = 53.84 ppm, $\delta(CDCl_3)$ = 77.16 ppm), or an external standard (^{31}P: 85% aqueous H_3PO_4 in sealed capillary; ^{19}F: $CFCl_3$ in $CDCl_3$).[133−135] Signals were assigned with the help of DEPT-135 and two-dimensional correlation spectra ($^1H,^1H$-COSY, $^1H,^{13}C$-HSQC, and $^1H,^{13}C$-HMBC). Signal multiplicities are abbreviated as s (singlet), d (doublet), t (triplet), sept (septett), m (multiplet), and br. (broad signal).

The ^{55}Mn (I = 5/2) NMR experiments were performed on a 14.1 T instrument at a frequency of 148.56 MHz using a broad-band direct observe probe (BBFO). The transmitter offset was chosen as −1400 ppm and a spectral width of 100 ppm (14.8 kHz) was applied. The 90° pulse was 13 μs at a power level of 100 W. We used a 90° excitation mode, an acquisition time of 2.0 s, and a recycling delay of 100 ms. Sixty four scans were acquired and multiplied with an exponential line broadening function (lb = 5 Hz) before Fourier transformation. The ^{55}Mn chemical shifts were referenced to a saturated solution of $KMnO_4$ in D_2O as δ = 0.00 ppm.[136] The recommended reference concentration of 0.82 mol kg^{-1} (13% w/w) is more than twice higher than the solubility in water at room temperature and seems incorrect.

Elemental analyses were performed using a vario MICRO cube CHN element analyzer from Elementar. Samples were burned in sealed tin containers using a stream of oxygen.

High-resolution ESI mass spectra were recorded on a Bruker maXis 4G ESI-Q-TOF spectrometer under direct injection conditions with CH_3CN as a solvent.

IR spectra were recorded on a Shimadzu IRTracer-100 with QATR 10 spectrometer. Signal intensities are marked as vs (very strong), s (strong), m (medium), w (weak), br (broad), and vw (very weak).

X-ray powder diffraction (XRPD) measurements were performed with a STOE STADI P diffractometer with a microfocused Cu Kα radiation source (λ = 1.542 Å) equipped with a DECTRIS MYTHEN 1K detector.

Cyclic voltammetry was performed using a Versastat4-200 potentiostat from Princeton Applied Research in a glovebox. A glassy carbon disk electrode served as a working electrode, and two silver wires served as counter and pseudo-reference electrodes. Ferrocene was added as an internal reference ($E_{1/2}$ vs saturated calomel electrode (SCE) in dichloromethane (DCM) = 0.475 V).[137] The solvent was dry and deaerated CH_2Cl_2 with 0.1 M $TBAPF_6$ (tetra-*n*-butylammonium hexafluorophosphate) as an electrolyte. Potential sweep rates were, unless otherwise stated, 100 mV s^{-1}.

All photophysical measurements were performed, unless otherwise stated, under an Ar atmosphere in either Schlenk or screw cap cuvette with dry and argon-saturated solvents (CH_3CN and CH_2Cl_2).

UV/vis absorption spectroscopy was performed using a Cary 5000 instrument from Varian.

For photostability experiments, a Flame UV/vis spectrometer system from Ocean optics was used with a continuous-wave (cw) laser from Roithner Lasertechnik emitting at 405 nm (optical output up to 375 mA and 526 mW, circular beam dimension with a diameter of 2.5 mm) and a cw-laser emitting at 447 nm (optical output up to 1050 mA and 1.1 W, rectangular beam dimension with a diameter of 2 × 5 mm^2). Spectroscopic experiments with that cw-laser as a light source were carried out at 293 K using self-built cuvette holders allowing temperature control and stirring of the solution with a small magnetic stir bar. Photochemical processes involving free radicals and triplet-excited states are usually sensitive to dissolved oxygen. Therefore, oxygen was removed by saturating the solution with argon (for 5 min) before the measurements.

2.2. Single-Crystal X-ray Structure Analysis. $[Mn(CNdippPh^{OMe2})_6]PF_6$ was recrystallized from DCM and cyclohexane at room temperature. Single yellow block-shaped crystals were obtained after a few days. A suitable crystal with dimensions 0.20 × 0.16 × 0.12 mm^3 was selected, and the crystal was mounted on a mylar loop in perfluoroether oil on a Cu-Stoe diffractometer. The crystal was kept at a steady T = 150 K during data collection. The structure was solved with the olex2.solve 1.5[138] solution program using iterative methods and using Olex2 1.5[139] as the graphical interface. The model was refined with ShelXL 2018/3[140] using full-matrix least-squares minimization on F2.

Crystallographic drawings were made with the software packages Mercury[141,142] and CYLview.[143] Selected crystal data and details of the structure determinations are presented in Tables S1 and S2.

CCDC-2165895 ($[Mn(CNdippPh^{OMe2})_6]PF_6$ at 150 K) contains the supplementary crystallographic data for this article. These data can be obtained free of charge from the Cambridge Crystallographic Data Centre via http://www.ccdc.cam.ac.uk/data_request/cif.[144−146]

2.3. Density Functional Theory (DFT) Calculations. All calculations were carried out for the gas phase using the ORCA 4.1.2 package.[147−149] Geometry optimization and the calculation of infrared modes were performed with the composite approach PBEh-3c,[150] the basis def2-mSVP(C,H,N,O)[150] and def2-mTZVP(Mn)[151] with the atom pairwise dispersion correction with the Becke−Johnson damping scheme (D3BJ),[152,153] the geometrical counterpoise correction gCP,[154] the RIJCOSX approximation, the auxiliary basis def2/J,[155] fine numerical integration grids (grid5, gridX7, and NoFinalGrid in ORCA 4 nomenclature), and KDIIS+SOSCF. The

https://doi.org/10.1021/acs.inorgchem.2c01438
Inorg. Chem. 2022, 61, 10533−10547

Scheme 1. Synthesis of $[Mn(CNdippPh^{OMe2})_6]PF_6$

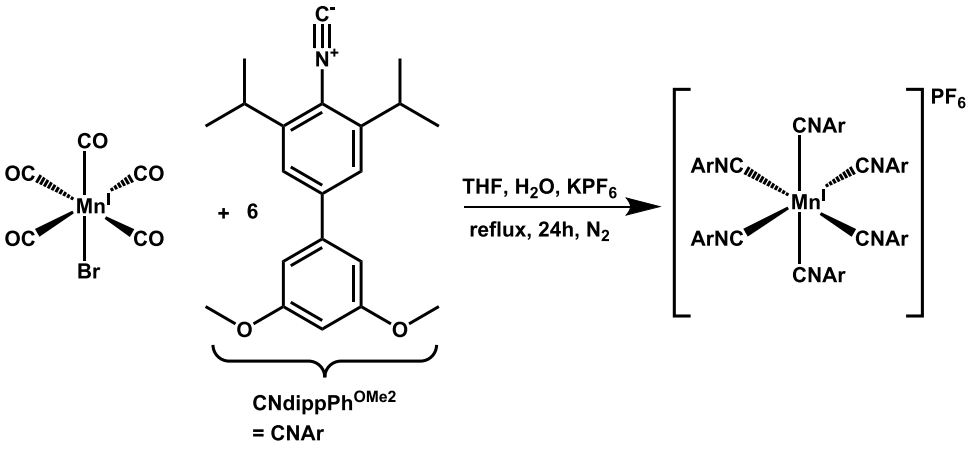

crystallographic structure of the complex was used as a starting point. The libint2 library was used for the computation of 2-el integrals.[156] The calculated frequencies were scaled by a factor of 0.95.[150] No imaginary frequencies were obtained. Calculations were performed without symmetry. The Cartesian coordinates from the geometry optimization are in the Supporting Information (SI). The output results were handled with the ChemCraft software package.[157]

2.4. General Synthesis Procedures and Product Characterizations. The synthesis and characterization of the ligand $CNdippPh^{OMe2}$ is described in the SI (see Schemes S1 and S2). The complexation was carried out in dry solvents and under a nitrogen atmosphere using standard Schlenk techniques. $[Mn(CO)_5Br]$ and KPF_6 were purchased and used without further purification. THF was purified by a solvent purification system (SPS) by Innovative Technology and further degassing by at least three cycles of the freeze−pump−thaw method using nitrogen.

Synthesis of $[Mn(CNdippPh^{OMe2})_6]PF_6$. $[Mn(CO)_5Br]$ (20.4 mg, 72.7 μmol) and $CNdippPh^{OMe2}$ (141 mg, 436 μmol) were dissolved in dry and degassed THF (5 mL) and refluxed for 24 h. After cooling to room temperature, a saturated aqueous solution of KPF_6 (5−10 mL) was added. Overnight, a bright yellow to orange solid formed. The precipitate was collected by suction filtration and washed with deionized water. The solid was dissolved in DCM, dried over Na_2SO_4, filtered off, and washed with DCM. The solvent was removed in vacuum, resulting in an orange solid. This solid was recrystallized in DCM and cyclohexane at room temperature. Yellow crystals were obtained after a few days. The crystals were filtered off and dried under air, leading to a yellow powder. Yield: 82 mg (38.3 μmol, 53% relative to $[Mn(CO)_5Br]$).

Elemental analysis calculated for $C_{126}H_{150}F_6MnN_6O_{12}P$: C 70.70, H 3.93, N 7.06%, found: C 70.41, H 3.62, N 6.68%.

HR-ESI-MS(+)(CH_3CN): m/z (%) = $[M - PF_6]^+$ calcd 1995.0720, found 1995.0679 (100), $[M - PF_6 - L + CH_3CN]^+$ calcd 1712.9106, found 1712.9063 (36), $[M - PF_6 - L + CO]^+$ calcd 1699.8790, found 1699.8749 (20.9).

^1H NMR (600 MHz, CD_2Cl_2): δ/ppm = 7.42 (s, 2H, $\{(Me_2CH)_2C_6\underline{H}_2(C_6H_3OMe_2)(NC)\}_6Mn$), 6.74 (d, $^3J_{H-H}$ = 2.3 Hz, 2H, $\{(Me_2CH)_2C_6H_2(C_6\underline{H}_3OMe_2)(NC)\}_6Mn$), 6.51 (t, $^3J_{H-H}$ = 2.2 Hz, 1H, $\{(Me_2CH)_2C_6H_2(C_6\underline{H}_3OMe_2)(NC)\}_6Mn$), 3.86 (s, 6H, $\{(Me_2CH)_2C_6H_2(C_6H_3O\underline{Me}_2)(NC)\}_6Mn$), 3.43 (sept, $^3J_{H-H}$ = 6.9 Hz, 2H, $\{(Me_2C\underline{H})_2C_6H_2(C_6H_3OMe_2)(NC)\}_6Mn$), 1.23 (d, $^3J_{H-H}$ = 7.0 Hz, 12H, $\{(\underline{Me}_2CH)_2C_6H_2(C_6H_3OMe_2)(NC)\}_6Mn$).

$^{13}C\{^1H\}$ NMR (151 MHz, CD_2Cl_2): δ/ppm = 176.0−182.0 (m, C_q, $\{(Me_2CH)_2C_6H_2(C_6H_3OMe_2)(N\underline{C})\}_6Mn$), 161.7 ($C_q$, $\{(Me_2CH)_2C_6H_2(\underline{C}_6H_3OMe_2)(NC)\}_6Mn$), 145.0 ($C_q$, $\{(Me_2CH)_2\underline{C}_6H_2(C_6H_3OMe_2)(NC)\}_6Mn$), 142.6 ($C_q$, $\{(Me_2CH)_2\underline{C}_6H_2(\underline{C}_6H_3OMe_2)(NC)\}_6Mn$), 142.1 ($C_q$, $\{(Me_2CH)_2\underline{C}_6H_2(\underline{C}_6H_3OMe_2)(NC)\}_6Mn$), 125.3 ($C_q$, $\{(Me_2CH)_2\underline{C}_6H_2(C_6H_3OMe_2)(NC)\}_6Mn$), 122.9 (CH, $\{(Me_2CH)_2\underline{C}_6H_2(C_6H_3OMe_2)(NC)\}_6Mn$), 106.1 (CH, $\{(Me_2CH)_2C_6H_2(\underline{C}_6H_3OMe_2)(NC)\}_6Mn$), 99.5 (CH, $\{(Me_2CH)_2C_6H_2(\underline{C}_6H_3OMe_2)(NC)\}_6Mn$), 55.9 ($CH_3$, $\{(Me_2CH)_2C_6H_2(C_6H_3O\underline{Me}_2)(NC)\}_6Mn$), 31.0 (CH, $\{(Me_2\underline{C}H)_2C_6H_2(C_6H_3OMe_2)(NC)\}_6Mn$), 22.6 ($CH_3$, $\{(\underline{Me}_2CH)_2C_6H_2(C_6H_3OMe_2)(NC)\}_6Mn$).

^{55}Mn NMR (148.5 MHz, CD_2Cl_2): δ/ppm = −1389.52 (s, Mn).

^{19}F NMR (565 MHz, CD_2Cl_2): δ/ppm = −73.68 (d, J = 710.2 Hz, PF_6^-).

^{31}P NMR (243 MHz, CD_2Cl_2): δ/ppm = −144.54 (sept, J = 710.2 Hz, PF_6^-).

Ir (ATR, 298 K): υ/cm^{-1} = 3075 (w, υ[=C−H]), 2964 (m, υ[−C−H]), 2932 (m, υ[−C−H]), 2875 (w, υ[−C−H]), 2846 (w, υ[−C−H]), 2070 (s, υ[−N≡C]), 1592 (s), 1573 (w), 1457 (m), 1434 (m), 1403 (m), 1386 (w), 1355 (m), 1324 (w), 1310 (w), 1266 (m), 1203 (s), 1153 (s), 1133 (w), 1111 (w), 1064 (m), 1038 (m), 992 (w), 962 (w), 943 (w), 928 (w), 904 (w), 891 (w), 877 (w), 836 (vs, $\nu[PF_6]$), 788 (s), 757 (m), 735 (m), 697 (m), 660 (w), 586 (vs), 556 (m), 525 (w), 480 (w), 464 (w).

The experimental XRPD pattern as well as the calculated pattern obtained from the single-crystal structure are shown in Figure S7. Not surprisingly, the XRPD pattern of the single-crystal structure containing 0.8 water and 2 cyclohexane molecules per unit cell does not match the XRPD pattern of the yellow powder of $[Mn(CNdippPh^{OMe2})_6]PF_6$ because of the loss of solvent by drying the crystals under air.

3. RESULTS AND DISCUSSION

3.1. Synthesis, Characterization, Crystal Structure, and DFT Calculations. The ligand 4-(3,5-dimethoxyphenyl)-2,6-diisopropylphenylisocyanide ($CNdippPh^{OMe2}$) was synthesized following a previously published procedure,[103] which was adapted with modifications inspired by other studies (Schemes S1 and S2).[158,159] The complex was prepared by reacting 6 equiv of the monodentate isocyanide ligand $CNdippPh^{OMe2}$ with $[Mn(CO)_5Br]$ in THF under reflux and inert gas for 24 h (Scheme 1). Afterward, the complex was precipitated with an aqueous hexafluorophosphate solution and yellow crystals were obtained from DCM/cyclohexane. As a solid, the compound $[Mn(CNdippPh^{OMe2})_6]PF_6$ can be handled under an ambient atmosphere without noticeable degradation, and ^1H, ^{13}C, ^{19}F, and ^{31}P NMR spectra in deuterated DCM confirm that the compound is pure (Figures S1−S5). The ESI-HR measure-

https://doi.org/10.1021/acs.inorgchem.2c01438
Inorg. Chem. 2022, 61, 10533−10547

ments in CH_3CN exhibit the expected mass peak for $[M - PF_6]^+$ as well as the mass peaks for $[M - PF_6 - L + CH_3CN]^+$ and $[M - PF_6 - L + CO]^+$ (Figure S8 and Table S3). Over time, the solution stored under ambient conditions and ambient light becomes intensely yellow colored, and measurements performed after a few days exhibit the mass peaks for $[M - PF_6 - L + CH_3CN]^+$, $[M - PF_6 - 2L + 2CH_3CN]^+$, $[M - PF_6 - 3L + 2O]^+$, and $[M - PF_6 - 4L + 2O]^+$, along with some additional minor mass peaks (Figure S9 and Table S3). Evidently, ligand exchange occurs in coordinating CH_3CN solvent over time, and furthermore, the presence of oxygen seems to be detrimental.

In the ^{13}C NMR spectrum of $[Mn(CNdippPh^{OMe2})_6]PF_6$ in CD_2Cl_2 (Figures S2 and S3), the coordinating C-atoms of the aromatic isocyanide ligands appear between 170 and 185 ppm in the form of a multiplet, likely reflecting an overlay of ^{55}Mn ($I = 5/2$) and ^{14}N ($I = 1$) coupling patterns. This finding fits perfectly with the previously reported three compounds $[Mn(CNPh)_6]BF_4$, $[Mn(CNPh^{para-Me})_6]BF_4$, and $[Mn(CNPh^{p-OMe})_6]BF_4$ in CD_3CN, which exhibit identical signals in the chemical shift range from 170 to 185 ppm.[160]

The ^{55}Mn NMR spectrum in CD_2Cl_2 (Figure S6) exhibits a remarkably sharp resonance at -1390 ppm with a linewidth (fwhh) of only 69 Hz, in line with an almost perfect O_h symmetry of the primary coordination sphere around Mn. The observable chemical shift is in the expected range for Mn(I) between -1000 ppm and -1500 ppm and thus confirms the +I oxidation state. This signal is not changing over a few hours in CD_2Cl_2 at 298 K in the dark, hence ligand exchange is evidently slower in this solvent than in CH_3CN. The chemical shift observed for $[Mn(CNdippPh^{OMe2})_6]^+$ (−1390 ppm) lies between the values found for our two previously investigated manganese(I) complexes with chelating arylisocyanides,[54] which featured ^{55}Mn resonances at -1225 and -1419 ppm, suggesting that the new complex has an electron density at Mn(I) somewhere in between the two previously studied related compounds. More striking is the very large difference in linewidth associated with the ^{55}Mn resonances, which is only 69 Hz for $[Mn(CNdippPh^{OMe2})_6]^+$ but amounts to 2100 Hz and 5900 Hz in the previously studied chelate complexes, and this reflects the higher symmetry of the new Mn(I) complex with monodentate arylisocyanide ligands. Furthermore, this finding of a relatively narrow ^{55}Mn resonance bandwidth is similar to the abovementioned other Mn(I) complexes with monodentate arylisocyanide ligands of the type $[Mn(CNR)_6]BF_4$. For example, $[Mn(CNPh)_6]BF_4$ featured its ^{55}Mn resonance at -1382 ppm with a linewidth of 42 Hz in CD_3CN at 18 °C.[160]

An additional resonance at -1387 ppm is observable in the ^{55}Mn NMR spectrum of $[Mn(CNdippPh^{OMe2})_6]PF_6$ (Figure S6), but its integral is more than 10 times lower than that of the main resonance at -1389 ppm. We tentatively attribute the minor resonance at −1387 ppm to $[Mn(CO)(CNdippPh^{OMe2})_5]PF_6$, the mass peak of which is furthermore observable in the high-resolution electrospray ionization mass spectrometry (HR-ESI-MS) measurements.

The compound $[Mn(CNdippPh^{OMe2})_6]PF_6$ crystallizes in the $P\bar{1}$ space group with $Z = 1$ molecule in the unit cell. The obtained crystal structure contains 0.8 water and 2 cyclohexane molecules per formula unit. The asymmetric unit consists of the manganese cation, three $CNdippPh^{OMe2}$ ligands, and the PF_6^- anion. The Mn(I) cation is coordinated by six neutral $CNdippPh^{OMe2}$ ligands (Figure 1). The Mn−C bond distances

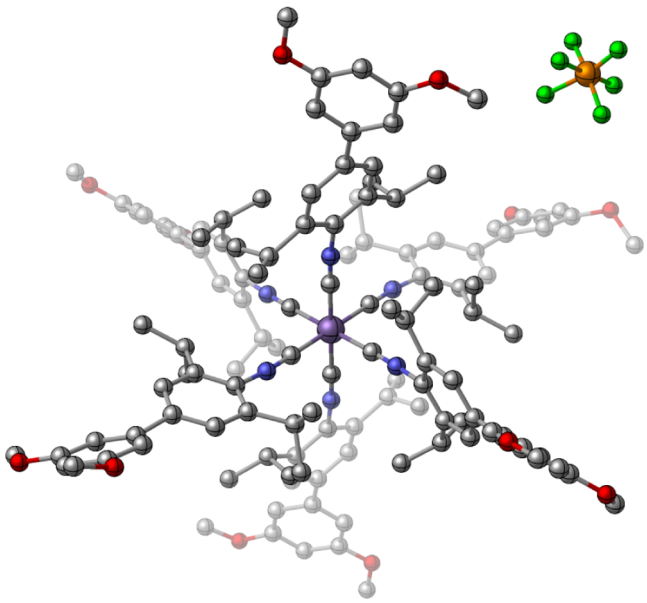

Figure 1. Crystal structure of $[Mn(CNdippPh^{OMe2})_6]PF_6$. Hydrogen atoms and solvents (H_2O and cyclohexane) are omitted for clarity. Color Code: C (gray), O (red), N (blue), Mn (purple), F (green), and P (orange).

are between 1.878(8) and 1.881(7) Å at 150 K (Table S2). The slightly distorted octahedral geometry is evident from the small differences in Mn−C bond lengths and the small deviations in the C−Mn−C bond angles from 90° (Table S2). For a more quantitative analysis of the deviation from perfect octahedral symmetry, we employed the Σ and Θ parameters, where Σ is a general measure for the deviation from ideal octahedral geometry and Θ quantifies the distortion from an octahedral toward a trigonal prismatic structure (eq S1 and Table S2).[161−163] A perfectly octahedral complex would give Σ = Θ = 0.[161−163] From the crystal structure of $[Mn(CNdippPh^{OMe2})_6]PF_6$, we obtain Σ = 22.55° and Θ = 58.37°, relatively close to O_h symmetry. For reference, the $[Mn(CNPh)_6]I_3$ compound has Σ = 25.84° and Θ = 65.51° (Table S2).[164] Furthermore, the structure of $[Mn(CNdippPh^{OMe2})_6]PF_6$ is also somewhat less distorted than the analogous W(0) complex $[W(CNdippPh^{OMe2})_6]$ (Σ = 26.52° and Θ = 66.33°, Table S2).[103]

The DFT geometry optimization of $[Mn(CNdippPh^{OMe2})_6]PF_6$ (PBEh-3c/def2-mSVP(C,H,N,O)/def2-mTZVP(Mn)) yields similar Mn−C bond lengths as the X-ray crystal structure (Table S2). Furthermore, the DFT-optimized geometry features a similar deviation from ideal octahedral geometry as the X-ray crystal structure (Σ = 20.83° and Θ = 56.41°, Table S2).

$[Mn(CNdippPh^{OMe2})_6]PF_6$ can be isolated as a yellow crystalline powder by filtration and subsequent drying under air. Not surprisingly, the experimental XRPD pattern of that yellow crystalline powder does not match the calculated X-ray pattern based on the single-crystal structure (Figure S7), due to the loss of crystal solvents during filtration and air drying. Combustion analysis of the crystalline yellow powder confirms that it is solvent-free.

3.2. Vibrational Spectroscopy and DFT Analysis. Infrared spectra of the complex and the free ligand were measured in the range of 400−3500 cm^{-1} (Figure 2). The C≡N stretching frequency (ν(C ≡ N)) of isocyanides is usually

https://doi.org/10.1021/acs.inorgchem.2c01438
Inorg. Chem. 2022, 61, 10533−10547

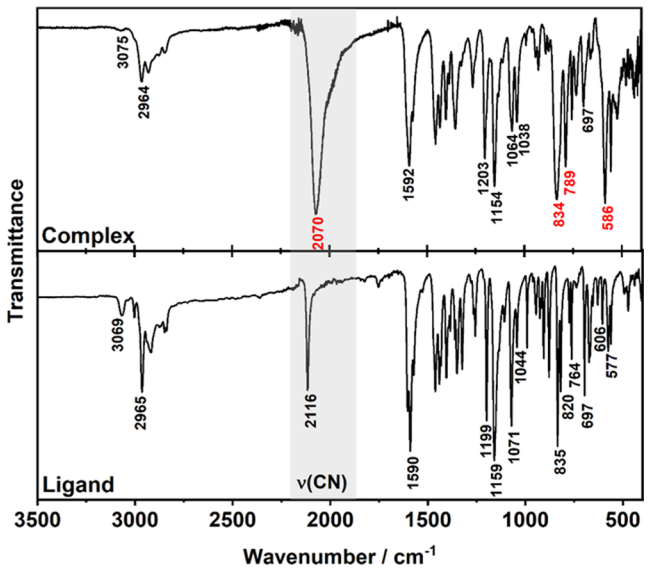

Figure 2. Solid-state ATR-IR spectra of the compound [Mn(CNdippPh^{OMe2})$_6$]PF$_6$ (top) and the free ligand (**4**) (bottom). The red marked frequencies of the complex are assigned in Table 1.

strongly influenced by the metal coordination,[47,53,54,158,165−180] and this is also the case here. In the IR spectrum of the free ligand, υ(C≡N) is observed at 2116 cm^{-1}, which is nearly the same for the analogous W-complex (2115 cm^{-1}), whereas in the complex [Mn(CNdippPh^{OMe2})$_6$]PF$_6$, it is shifted to 2070 cm^{-1}, due to π-backbonding from the metal center to the π^* antibonding orbital of the isocyanide moiety. Furthermore, the respective IR band is significantly broader in the complex than in the free ligand, presumably due to the somewhat distorted octahedral coordination geometry resulting in slightly different metal−ligand bond lengths and angles (Table S2), and consequently to a continuum of slightly differing vibrational frequencies (see below). Another explanation for the broadening could be the fact that the symmetry of the vibrational band in the complex is T_{1u}, whereas in the free ligand the symmetry is simply A. Two prominent IR bands at 586 and 789 cm^{-1} appearing in the spectrum of the complex but not in the free ligand are tentatively attributed to Mn(I)-C vibrational modes, in analogy to a recently explored isoelectronic Cr(0) arylisocyanide complex, where the Cr(0)−C vibration appeared at 590 cm^{-1}.[67]

For an ideal octahedral complex of the type [Mn−(C≡−N−C(Ar))$_6$], six IR-active T_{1u} modes are expected (υ(C≡N), υ(Mn−C), υ(N-C(Ar)), δ(Mn−C≡N), δ(C−Mn−C), and δ(C≡N-C(Ar))).[179] The infrared spectrum was analyzed only in terms of [Mn(−C≡N)] core vibrations (Table 1). The core vibrations of [Mn(CNdippPh^{OMe2})$_6$]$^+$ were obtained from DFT calculations (PBEh-3c/def2-mSVP(C,H,N,O)/def2-mTZVP(Mn)) (Figures S11−S14) and compared with the

Table 1. Selected Infrared Vibrational Frequencies for [Mn(CNdippPh^{OMe2})$_6$]PF$_6$ (Red Marked Frequencies in Figure 2) in Comparison with DFT Calculated Frequencies (PBEh-3c/def2-mSVP(C,H,N,O)/def2-mTZVP(Mn))[a] Scaled by a Factor of 0.95[150,b]

complex	mode	IR$_{exp}$[c] (cm^{-1})	IR$_{DFT}$ (cm^{-1})
[Mn(CNdippPh^{OMe2})$_6$]PF$_6$	υ(C≡N) T_{1u}	2070	2176 (2973), 2181 (2863), 2184 (1231)[d] and 2184 (2134)[d]
	υ(C≡N) E_g		2184 (1231),[d] 2184 (2134)[d] and 2188 (218)
	υ(C≡N) A_{1g}		2261 (1.07)
	PF_6^-	834	
	υ(Mn−C) T_{1u}	789	789.72 (118), 789.77 (121) and 790.38 (118)
	υ(Mn−C) E_g		792.46 (0.29) and 792.70 (1.66)
	υ(Mn−C) A_{1g}		793.12 (0.71)
	δ(C−Mn−C) and δ(Mn−C≡N) T_{1u}	586	599.57 (99), 601.19 (169), 608.21 (41), 610.13 (168), 613.87 (91) and 618.43 (131)
[Mn(L^{tri})$_2$]PF$_6$[54,e]	υ(C≡N) T_{1u}	2081	
	Mn−C	584	
[Mn(L^{bi})$_3$]PF$_6$[54,f]	υ(C≡N) T_{1u}	2064	
	Mn−C	568	
[Mn(CNPh)$_6$]PF$_6$[47]	υ(C≡N) T_{1u}	2088 (vs)	
	PF_6^-	840 (m)	
[Mn(CNPh)$_6$]I/Br/Cl[47]	υ(C≡N) T_{1u}	2088 (vs)	
[Mn(CNPh)$_6$]Cl[53]	υ(C≡N) T_{1u}	2080[g]	
[Mn(CNPh)$_6$]BF$_4$[173]	υ(C≡N) T_{1u}	2084	
[Mn(CNPh)$_6$]I[179]	υ(C≡N) T_{1u}[h]	2085 (vs) and 1993 (sh)	
	υ(N(isocyanide)-C(pheny)) T_{1u}[h]	1210	
	δ(Mn−C≡N) T_{1u}[h]	600 (vs)	
	υ(Mn−C) T_{1u}[h]	297 and 319 (multiplet)[i]	
	δ(C−Mn−C) T_{1u}[h]	113 (w)	

[a]The intensities of the vibrational frequencies obtained from DFT calculations (PBEh-3c/def2-mSVP(C,H,N,O)/def2-mTZVP(Mn)) are indicated in parentheses. (Abbreviations: bend., bending; str., stretching; ip, in-plane). [b]IR data from previously reported comparable compounds are included for comparison. [c]of the solid state. [d]One T_{1u} and E_g modes are mixed together at 2184 cm^{-1} leading to two IR observable modes. [e]L^{tri} = 5,5′-(2-isocyano-5-methyl-1,3-phenylene)bis(2-(3,5-di-*tert*-butyl-2-isocyanophenyl)thiophene). [f]L^{bi} = 2,5-bis(3,5-di-*tert*-butyl-2-isocyanophenyl)thiophene. [g]The peak shows a shoulder at lower wavenumbers.[53] [h]Approximated local symmetry O_h.[179] [i]Due to a breakdown of the T_{1u} degeneracy.[179]

https://doi.org/10.1021/acs.inorgchem.2c01438
Inorg. Chem. 2022, 61, 10533−10547

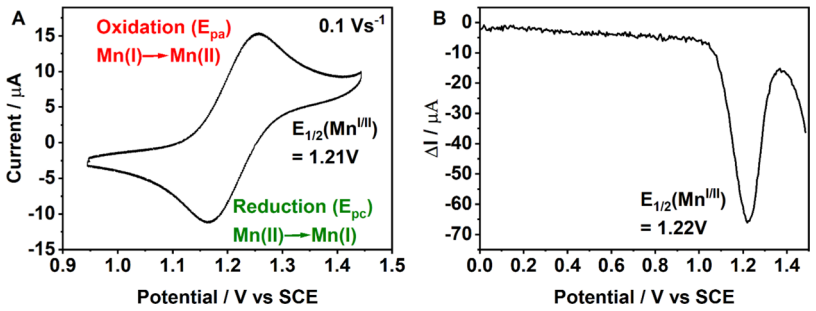

Figure 3. (A) Cyclic voltammogram for the Mn(I)/Mn(II) redox couple of $[Mn(CNdippPh^{OMe2})_6]PF_6$ in dry and deaerated CH_2Cl_2 containing 0.1 M $TBAPF_6$ at 20 °C, recorded with a scan rate of 100 mV s^{-1}. (B) Differential pulse voltammetry for the same redox couple under identical conditions.

experimentally obtained frequencies (Table 1 and Figures S12−S14). In addition, we compared the assigned vibrational modes with previous reports.[47,53,54,173,179]

For the complex $[Mn(CNdippPh^{OMe2})_6]^+$ (approximated local symmetry O_h), two symmetrical Raman-active (A_{1g} and doubly degenerate E_g) and one asymmetrical IR-active (triply degenerate T_{1u}) metal−ligand stretching modes (υ(Mn−C)) are expected.[179,181,182] DFT vibrational analysis reveals a splitting of the IR-active υ(Mn−C) T_{1u} mode into three stretching modes with observable Mn motion in the *x*, *y*, and *z* directions for $[Mn(CNdippPh^{OMe2})_6]^+$ (Table 1 and Figures S12−S14) at 789.72, 789.77, and 790.38 cm^{-1}, probably because of the small deviation from an ideal octahedral symmetry (Table S2). These modes are forming one band at 790 cm^{-1} in a simulated IR spectrum (Figure S11).

A complex with O_h symmetry should furthermore exhibit one Raman-active (triply degenerate T_{2g}), one forbidden (triply degenerate T_{2u}), and one IR-active (triply degenerate T_{1u}) metal−ligand bending mode (δ(Mn−C≡N) as well as for δ(C−Mn−C)).[179,181,182] The calculations reveal between 599 and 618 cm^{-1} six-core vibration bending modes in *x*, *y*, and *z* directions with dominant Mn motions (Table 1). Specifically, these modes are at 599.57, 601.19, 608.21, 610.13, 613.87, and 618.43 cm^{-1}. It seems that these modes originate from the combination of the δ(Mn−C≡N) and δ(C−Mn−C) bending modes, related to the fact that the complex shows deviation from ideal octahedral geometry (Table S2). All computed modes form together one band at 610 cm^{-1} in a simulated IR spectrum (Figure S11) and correspond to the expected T_{1u} bending mode.

Finally, the υ(C≡N) T_{1u} mode is also split into a few IR-active motions in *x*, *y*, and *z* directions. The IR-active modes can be identified in DFT calculations at 2176 and 2181 as well as at 2184 and 2184 cm^{-1} due to a mixing of one T_{1u} and one E_g motion (Table 1 and see SI, Figures S12−S14). These modes are forming one intense broad band at 2181 cm^{-1} in a simulated IR spectrum (Figure S11) and correspond also to an expected T_{1u} stretching mode.

On the basis of these DFT results supported by literature reports, the most relevant vibrational modes observed experimentally for $[Mn(CNdippPh^{OMe2})_6]PF_6$ can be assigned (Table 1). The calculated T_{1u} modes are split into three components due to small deviations from the O_h symmetry but these splittings cannot be observed experimentally. The observed band at 2070 cm^{-1} is attributed to the υ(C≡N) T_{1u} mode, calculated to appear at ca. 2181 cm^{-1}. This assignment is in agreement with several similar manganese(I) isocyanide complexes, which exhibit this mode between 2064 and 2088 cm^{-1}.[47,53,54,173,179] The respective IR band exhibits a weak shoulder at lower wavenumbers, which is also reported in the literature, and which results from some deviation from linearity of the CNR axis at the N-atom.[53,179] The X-ray crystal structure of $[Mn(CNdippPh^{OMe2})_6]PF_6$ shows that such a distortion is indeed present in the solid state. Alternatively, the respective IR shoulder could stem from a CO vibration of $[Mn(CO)(CNdippPh^{OMe2})_5]PF_6$, for which the ^{55}Mn NMR spectrum in Figure S6 provides some evidence (see above). The prominent broad band at 834 cm^{-1} is attributable to the PF_6^- anion, supported also by the fact that for $[Mn(CNPh)_6]PF_6$ this frequency is reported at 840 cm^{-1}.[47] The υ(Mn−C), δ(Mn−C≡N), and δ(C−Mn−C) T_{1u} modes resulting from the octahedral coordination skeleton of $[Mn(CNdippPh^{OMe2})_6]PF_6$ are observed at 789 and 586 cm^{-1} and can be assigned to the calculated IR-active T_{1u} modes at ca. 790 (υ(Mn−C) T_{1u}) and ca. 610 (δ(Mn−C≡N) and δ(C−Mn−C) T_{1u}) cm^{-1}. In the two previously investigated manganese(I) complexes with bidentate and tridentate isocyanides ligands, Mn−C vibrations at 568 and 584 cm^{-1} were found.[54] For $[Mn(CNPh)_6]I$, splitting into the two T_{1u} bending modes δ(Mn−C≡N) (600 cm^{-1}) and δ(C−Mn−C) (113 cm^{-1}) was reported.[179] As mentioned above, in our calculations, these two modes appear together around 610 cm^{-1} (see gifs in the SI).

3.3. Electrochemistry. The cyclic voltammogram of $[Mn(CNdippPh^{OMe2})_6]PF_6$ in dry and deaerated CH_2Cl_2 containing 0.1 M $TBAPF_6$ shows an oxidation wave at 1.21 V vs SCE ($E_{1/2}$), which can be attributed to the one-electron oxidation of Mn(I) to Mn(II) (Figure 3A). A value of $E_{1/2}$ = 1.22 V was determined by differential pulse voltammetry (Figure 3B). In the potential range between 0 and −2.3 V vs SCE (Figure S15), no redox waves are detectable, and thus the reduction potentials of the coordinated ligands cannot be determined under these conditions. $[Mn(CNdippPh^{OMe2})_6]PF_6$ undergoes a second one-electron oxidation at $E_{1/2}$ = 1.74 V vs SCE, likely attributable to the redox couple Mn(II/III) (Figure S15). The shape of the wave in Figure 3A and the peak−current ratio indicate a quasi-reversible chemical and electrochemical process. The difference between the anodic (E_{pa}) and cathodic (E_{pc}) peak potentials (peak-to-peak separation, ΔE_p) is 92 mV (at a scan rate of 100 mV s^{-1}) instead of the expectable 57 mV for a one-electron process at 25 °C, and the ratio of the anodic and cathodic peak currents is not equal to one ($|I_{pa}/I_{pc}| \neq 1$).[183]

To investigate the electrochemical reversibility of the single electron transfer process at 1.21 V in more detail, the cyclic voltammogram was measured at different scan rates (Figure

https://doi.org/10.1021/acs.inorgchem.2c01438
Inorg. Chem. 2022, 61, 10533−10547

S16A), and the respective data were used to make a Randles–Ševcík plot (Figure S16B).[183] The observed slight deviation from linearity in the plots of I_{pa} and I_{pc} vs $v^{1/2}$ (Figure S16B) suggests electrochemical quasi-reversibility, further confirmed by the observation that the peak-to-peak separation gets larger with increasing potential scan rate (see Trumpet plot in Figure S17).

In $[Mn(CNPh)_6]PF_6$, the quasi-reversible oxidation of Mn(I) to Mn(II) occurs at 1.01 V vs SCE in CH_2Cl_2 (Table 2).[46,50] The $E_{1/2}$ value of $[Mn(CNPh)_6]PF_6$ is close to the

Table 2. Electrochemical Potentials of $[Mn(CNdippPh^{OMe2})_6]PF_6$ in Comparison with Similar Compounds from the Literature

compound	$E_{1/2}$ ($Mn^{I/II}$) vs SCE (V)	$E_{1/2}$ ($Mn^{II/III}$) vs SCE (V)
$[Mn(CNdippPh^{OMe2})_6]PF_6$[a]	1.21	1.74[b]
$[Mn(L^{tri})_2]PF_6$[54 a,c]	1.00	
$[Mn(L^{bi})_3]PF_6$[54 a,d]	1.05	
$[Mn(CNPh)_6]PF_6$[46 e]	1.01	1.91
$[Mn(CNMe)_6]PF_6$[46 e]	0.47	1.59

[a]In (dry and deaerated) CH_2Cl_2 at 20 °C with $TBAPF_6$ (0.1 M) as the supporting electrolyte. [b]Only observable during one cycle (irreversible). [c]L^{tri} = 5,5′-(2-isocyano-5-methyl-1,3-phenylene)bis(2-(3,5-di-*tert*-butyl-2-isocyanophenyl)thiophene). [d]L^{bi} = 2,5-bis(3,5-di-*tert*-butyl-2-isocyanophenyl)thiophene. [e]In CH_2Cl_2 (5×10^{-3} M) with $TBAClO_4$ (0.1 M) as the supporting electrolyte.

Mn(I/II) potentials reported for our previously investigated $[Mn(L^{tri})_2]PF_6$ and $[Mn(L^{bi})_3]PF_6$ compounds (1.00 and 1.05 V vs SCE in CH_2Cl_2; L^{tri} = 5,5′-(2-isocyano-5-methyl-1,3-phenylene)bis(2-(3,5-di-*tert*-butyl-2-isocyanophenyl)-thiophene) and L^{bi} = 2,5-bis(3,5-di-*tert*-butyl-2-isocyanophenyl)thiophene).[54] In $[Mn(CNMe)_6]PF_6$, the oxidation of Mn(I) to Mn(II) occurs already at 0.47 V vs SCE in CH_2Cl_2 due to the stronger electron-donating character of the aliphatic isocyanide ligands compared to arylisocyanides.[46,50] For $[Mn(CNMe)_6]PF_6$ and $[Mn(CNPh)_6]PF_6$, a second one-electron wave was detected at 1.59 and 1.91 V vs SCE, respectively, and assigned to the oxidation of Mn(II) to Mn(III).[46] Against this background, it seems clear that the first and the second one-electron oxidation events observed for $[Mn(CNdippPh^{OMe2})_6]PF_6$ are metal-based and furthermore that the arylisocyanide ligand $CNdippPh^{OMe2}$ makes oxidation easier compared to the other discussed arylisocyanide manganese(I) complexes.

3.4. Optical Spectroscopy. The UV–vis spectrum of $[Mn(CNdippPh^{OMe2})_6]PF_6$ exhibits two absorption band maxima at 278 nm and 370 nm (Figure 4, blue line), similar to $[Mn(CNPh)_6]Cl$.[53] Thus, the yellow color stems from the broad absorption band maximizing at 370 nm, which tails into the violet region and which is not present in the UV–vis spectrum of the free ligand (Figure 4B, black trace). In CH_2Cl_2, the band at 278 nm has an extinction coefficient (ε) of 1.5×10^5 M^{-1} cm^{-1}, whereas the band at 370 nm shows a slightly lower ε-value of 1.4×10^5 M^{-1} cm^{-1}. For $[Mn(CNPh)_6]Cl$ in ethanol/methanol/diethyl ether (8:2:1), an absorption band at 225 nm ($\varepsilon = 7.5 \times 10^4$ M^{-1} cm^{-1}) with shoulders at 234 ($\varepsilon = 7.1 \times 10^4$ M^{-1} cm^{-1}) and 249 nm ($\varepsilon = 5.1 \times 10^4$ M^{-1} cm^{-1}) was assigned to an intraligand (IL) transition ($\pi \rightarrow \pi^*$), whereas a band centered at 322 nm ($\varepsilon = 6.6 \times 10^4$ M^{-1} cm^{-1}) with a shoulder at 340 nm ($\varepsilon = 6.1 \times 10^4$ M^{-1} cm^{-1}) was attributed to MLCT ($d\pi \rightarrow \pi^*$) transitions.[101] Our previously reported Mn(I) compounds $[Mn(L^{tri})_2]PF_6$ and $[Mn(L^{bi})_3]PF_6$ in CH_2Cl_2 showed absorption bands near 400 nm with similar extinction coefficients ($(2-4) \times 10^4$ M^{-1} cm^{-1}) and were likewise assigned to MLCT transitions.[54] Against this background, it seems plausible that the absorption band observable for $[Mn(CNdippPh^{OMe2})_6]PF_6$ at 278 nm is predominantly due to intraligand (IL) transitions ($\pi \rightarrow \pi^*$), whereas the band at 370 nm could be due to a delocalized MLCT or a mixed MLCT/IL transition.

Continuous photoexcitation into the band at 370 nm or into its tail at 410 nm causes a decrease of the absorption band at 370 nm and leads to the appearance of a shoulder near 425 nm, both in CH_3CN and in CH_2Cl_2 (green traces in Figure 4). This behavior is observable under laser irradiation (Figure 4A) as well as under illumination with the Xenon lamp of a commercial fluorimeter (Figure 4B), suggesting that photo-induced ligand dissociation occurs.

In contrast to our previously reported manganese(I)[54] and isoelectronic chromium(0)[66,67] complexes with chelating arylisocyanide ligands,[99] $[Mn(CNdippPh^{OMe2})_6]PF_6$ does not show any detectable photoluminescence, neither in solution at room temperature (both in CH_2Cl_2 and CH_3CN) nor at 77 K in a 2-methyl-THF glass. Consequently, we explored whether there are any dark (i. e., nonluminescent) states that could be detectable prior to the abovementioned photodecomposition. Light-induced ligand dissociation typically occurs from dissociative metal-centered excited states, and those states are usually nonemissive.[126,184−186] However, all our attempts to detect any such dark state with ns, ps, and fs laser transient absorption spectroscopy were unsuccessful. These findings are reminiscent of photoCORM behavior, such as observed, for

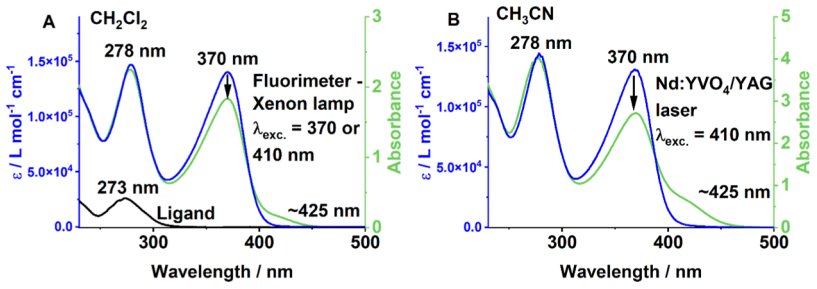

Figure 4. UV/vis absorption spectra of $[Mn(CNdippPh^{OMe2})_6]PF_6$ in dry and argon-saturated (A) CH_2Cl_2 and (B) CH_3CN before (blue) and after (green) irradiation with the Xenon lamp of (A) a spectrofluorometer or (B) a picosecond laser. The UV/vis spectrum of the free ligand in CH_2Cl_2 is included in (A). The absorbance axes (colored in green) apply to all measured spectra.

https://doi.org/10.1021/acs.inorgchem.2c01438
Inorg. Chem. 2022, 61, 10533−10547

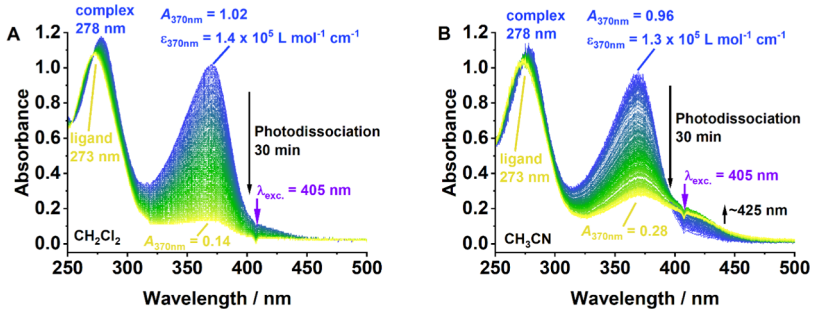

Figure 5. Photodegradation of (A) 7.29 μM [Mn(CNdippPh^{OMe2})$_6$]PF$_6$ in dry and argon-saturated CH_2Cl_2 and (B) 7.13 μM of the same compound in dry and argon-saturated CH_3CN upon irradiation with a cw-laser (405 nm, 526 mW) for 30 min. Time steps between each spectrum: 10 seconds. The dips at 405 nm in (A) and (B) are artefacts caused by the cw-laser (marked by λ_{exc} and purple arrows).

Table 3. Comparison of [Mn(CNdippPh^{OMe2})$_6$]PF$_6$ to Related Mn(I) Compounds with Tris(bidendate) and Bis(tridentate) Coordination Environments[a]

Compound	Ligand structure	UV/Vis λ_{max} [a]	υ(C≡N) T_{1u} / cm^{-1}
[Mn(CNdippPh^{OMe2})$_6$]PF$_6$	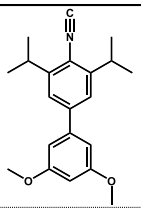	278 nm ($\varepsilon = 1.5 \cdot 10^5$ M^{-1} cm^{-1}) 370 nm ($\varepsilon = 1.4 \cdot 10^5$ M^{-1} cm^{-1})	2070
[Mn(L^{tri})$_2$]PF$_6$	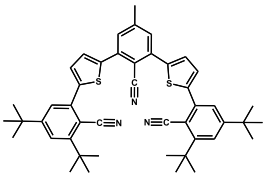	258 nm ($\varepsilon = 1.1 \cdot 10^5$ M^{-1} cm^{-1}) 327 nm ($\varepsilon = 0.65 \cdot 10^5$ M^{-1} cm^{-1}) 392 nm ($\varepsilon = 0.29 \cdot 10^5$ M^{-1} cm^{-1})	2081
[Mn(L^{bi})$_3$]PF$_6$	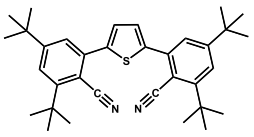	253 nm ($\varepsilon = 0.99 \cdot 10^5$ M^{-1} cm^{-1}) 308 nm ($\varepsilon = 0.81 \cdot 10^5$ M^{-1} cm^{-1}) 380 nm ($\varepsilon = 0.29 \cdot 10^5$ M^{-1} cm^{-1})	2064

[a]In CH_2Cl_2 at 20 °C.

example, in tricarbonyl manganese(I) complexes of the type [Mn(CO)$_3$(^{R}bpy)Br] (^{R}bpy = 4,4′-disubstituted-2,2′-bipyridyl ligand, where R = ^{t}Bu, H or CF_3).[184] Upon photoexcitation, these complexes undergo loss of one CO ligand on the femtosecond time scale, followed by solvent coordination on the picosecond time scale. The proposed mechanism of CO extrusion involves ultrafast internal conversion from an initially populated MLCT excited state to a dissociative ligand-field (d−d) excited state.[184]

3.5. Photoinduced Ligand Dissociation. To investigate the photodissociation in more detail, we irradiated [Mn(CNdippPh^{OMe2})$_6$]PF$_6$ in CH_2Cl_2 (Figures 5A and S18A) and in CH_3CN (Figure 5B) with a blue continuous-wave (cw) laser (405 nm, 526 mW). The absorbance at the excitation wavelength was adjusted close to 0.1 (Table S4), resulting in concentrations of 7.29 μM in CH_2Cl_2 (7.15 μM for a second measurement) and 7.13 μM in CH_3CN. The measurements were done at 25 °C and the absorption spectra were measured each 10 s during continuous irradiation at 405 nm.

Based on the series of UV−vis spectra in Figure 5, [Mn(CNdippPh^{OMe2})$_6$]$^+$ undergoes nearly complete photodegradation within 30 min. Aside from the very prominent absorbance decrease at 370 nm, the absorption band shift from 278 nm to 273 nm seems important, because the free ligand has an absorption band maximum at 273 nm (black trace in Figure 4A). Thus, the spectral evolution over time is compatible with the loss of one or more CNdippPh^{OMe2} ligands. Furthermore, in CH_3CN, a new absorption band at 425 nm becomes increasingly prominent with increasing irradiation time. When CH_2Cl_2 and CH_3CN solutions of

https://doi.org/10.1021/acs.inorgchem.2c01438
Inorg. Chem. 2022, 61, 10533−10547

$[Mn(CNdippPh^{OMe2})_6]PF_6$ are kept under ambient conditions without direct 405 nm irradiation, the UV−vis absorption spectra show comparatively minor changes over much longer time periods (Figure S19), compatible with the view that ligand loss is phototriggered. MS-ESI-HR measurements of a CH_3CN sample prior and after photoirradiation (Figure S10 and Table S3) show that the initially dominant $[M - PF_6]^+$ mass peak (relative intensity of 85% with respect to 100% for $[M - PF_6 - L + CH_3CN]^+$; L = $CNdippPh^{OMe2}$) vanishes with continuing irradiation, finally resulting in relative intensities of 4.3% for $[M - PF_6]^+$ and 64% for $[M - PF_6 - L + CH_3CN]^+$. Furthermore, a new mass peak attributable to $[M - PF_6 - 2L + 2CH_3CN]^+$ with a relative intensity of 15.7% becomes observable. Collectively, the irradiation experiments and HR-ESI-MS measurements demonstrate that light-induced ligand dissociation from an electronically excited state is much faster than spontaneous ligand dissociation in the electronic ground state.

The prototypical d^6 metal compound $[Ru(bpy)_3]^{2+}$ is known to undergo photodegradation as well,[4,187−189] and consequently it seemed meaningful to compare the photostabilities of $[Mn(CNdippPh^{OMe2})_6]PF_6$ and $[Ru(bpy)_3](PF_6)_2$ in CH_3CN under similar conditions (SI pages S27 to S31 and Figures S16B and S20 to S22). The key finding is that in CH_3CN our manganese(I) complex undergoes photodegradation far more efficiently than $[Ru(bpy)_3](PF_6)_2$ under these conditions of very intense cw-laser irradiation.

4. CONCLUSIONS

The primary coordination sphere of the $[Mn(CNdippPh^{OMe2})_6]^+$ complex comes close to O_h symmetry according to single-crystal X-ray diffraction, ^{55}Mn NMR spectroscopy, IR spectroscopy, and vibrational analysis with DFT calculations. A detailed vibrational analysis permitted the identification of the IR-active and asymmetrical $\upsilon(C{\equiv}N)$, $\upsilon(Mn{-}C)$, $\delta(C{-}Mn{-}C)$, and $\delta(Mn{-}C{\equiv}N)$ vibrational modes (T_{1u}), and furthermore reveals substantial differences in the π-backbonding interaction between the two previously investigated Mn(I) complexes with chelating isocyanide ligands and the new compound studied here (Table 3). Based on cyclic voltammetry, the Mn(I) center of $[Mn(CNdippPh^{OMe2})_6]PF_6$ is substantially more electron-rich than in previously reported hexakis(arylisocyanide)manganese(I) complexes.[46−52] Unlike our recently reported manganese(I) complexes with tris(bidendate) and bis(tridentate) coordination environments (Table 3),[54,99] and unlike its third-row congener $[W(CNdippPh^{OMe2})_6]$,[102−107] the $[Mn(CNdippPh^{OMe2})_6]^+$ complex is nonemissive. Instead, photoirradiation into its lowest energy UV−vis absorption band leads to ligand dissociation, similar to what is well-known from manganese(I) carbonyl compounds.[76,119−121,123,125−132] The much weaker ligand field in our $3d^6$ complex compared to that experienced by W(0) in the same coordination environment likely leads to fast and efficient population of a dissociative metal-centered excited state, which represents a common challenge in first-row transition metal compounds.[57,60] The photophysical properties of the new Mn(I) complex differ substantially from those of the recently reported analogous complexes with bi- and tridentate isocyanide ligands (Table 3).[54] Aside from the chelating nature of the previously used ligands, their thiophene units in the ligand skeleton likely affect the electronic structures of the resulting Mn(I) complexes.

Thus, our study suggests that monodentate isocyanide ligands are not well suited for obtaining manganese(I) complexes with emissive MLCT excited states. Chelating arylisocyanides, as used previously for chromium(0),[66,67] manganese(I) (Table 3),[54,99] and molybdenum(0),[158,190,191] seem better suited for this purpose.

■ ASSOCIATED CONTENT

Supporting Information

The Supporting Information is available free of charge at https://pubs.acs.org/doi/10.1021/acs.inorgchem.2c01438.

Synthesis procedures and characterization of the $CNdippPh^{OMe2}$ ligand; ^1H, ^{13}C, ^{19}F, ^{31}P, and ^{55}Mn NMR spectroscopy of $[Mn(CNdippPh^{OMe2})_6]PF_6$; crystallographic data and crystal structure of the complex; XRPD pattern; HR-ESI-MS measurements of the complex; IR spectra and vibrational analysis; and cyclic voltammetry measurements, photostability studies, and UV−vis absorption spectroscopy of the complex, as well as cartesian coordinates of the optimized structure of the complex (PDF)

Full dynamic figures of the corresponding metal−ligand vibrations (ZIP)

Accession Codes

CCDC 2165895 contains the supplementary crystallographic data for this paper. These data can be obtained free of charge via www.ccdc.cam.ac.uk/data_request/cif, or by emailing data_request@ccdc.cam.ac.uk, or by contacting The Cambridge Crystallographic Data Centre, 12 Union Road, Cambridge CB2 1EZ, UK; fax: +44 1223 336033.

CCDC-2165895 contains the supplementary crystallographic data for this paper. These data can be obtained free of charge via www.ccdc.cam.ac.uk/data_request/cif, or by emailing data_request@ccdc.cam.ac.uk, or by contacting The Cambridge Crystallographic Data Centre, 12 Union Road, Cambridge CB2 1EZ, UK; fax: +44 1223 336033.

■ AUTHOR INFORMATION

Corresponding Author

Oliver S. Wenger − *Department of Chemistry, University of Basel, 4056 Basel, Switzerland;* orcid.org/0000-0002-0739-0553; Email: oliver.wenger@unibas.ch

Authors

Sascha Ossinger − *Department of Chemistry, University of Basel, 4056 Basel, Switzerland*

Alessandro Prescimone − *Department of Chemistry, University of Basel, 4058 Basel, Switzerland;* orcid.org/0000-0002-3631-5210

Daniel Häussinger − *Department of Chemistry, University of Basel, 4056 Basel, Switzerland;* orcid.org/0000-0002-4798-0072

Complete contact information is available at: https://pubs.acs.org/10.1021/acs.inorgchem.2c01438

Author Contributions

The manuscript was written through contributions of all authors. All authors have given approval to the final version of the manuscript.

Notes

The authors declare no competing financial interest.

https://doi.org/10.1021/acs.inorgchem.2c01438
Inorg. Chem. 2022, 61, 10533−10547

Deutsche Forschungsgemeinschaft (DFG, German Research Foundation)—460752300. Swiss National Science Foundation—200021_178760.

■ ACKNOWLEDGMENTS

S.O. acknowledges funding from the Deutsche Forschungsgemeinschaft (DFG, German Research Foundation)—460752300 and by the University of Basel. O.S.W. thanks the Swiss National Science Foundation for funding through grant number 200021_178760. The authors thank S. Mittelheisser and J. Zurflüh for CHN measurements and M. Pfeffer for ESI mass spectrometry measurements. Calculations were performed at sciCORE (http://scicore.unibas.ch/) scientific computing center at the University of Basel.

■ REFERENCES

(1) Juris, A.; Balzani, V.; Barigelletti, F.; Campagna, S.; Belser, P.; von Zelewsky, A. Ru(II) Polypyridine Complexes: Photophysics, Photochemistry, Eletrochemistry, and Chemiluminescence. *Coord. Chem. Rev.* **1988**, *84*, 85−277.

(2) Hammarström, L.; Johansson, O. Expanded Bite Angles in Tridentate Ligands. Improving the Photophysical Properties in Bistridentate Ru^{II} Polypyridine Complexes. *Coord. Chem. Rev.* **2010**, *254*, 2546−2559.

(3) Hu, K.; Sampaio, R. N.; Schneider, J.; Troian-Gautier, L.; Meyer, G. J. Perspectives on Dye Sensitization of Nanocrystalline Mesoporous Thin Films. *J. Am. Chem. Soc.* **2020**, *142*, 16099−16116.

(4) Soupart, A.; Alary, F.; Heully, J. L.; Elliott, P. I. P.; Dixon, I. M. Theoretical Study of the Full Photosolvolysis Mechanism of $[Ru(Bpy)_3]^{2+}$: Providing a General Mechanistic Roadmap for the Photochemistry of $[Ru(N\wedge N)_3]^{2+}$-Type Complexes toward Both Cis and Trans Photoproducts. *Inorg. Chem.* **2020**, *59*, 14679−14695.

(5) Arias-Rotondo, D. The Fruit Fly of Photophysics. *Nat. Chem.* **2022**, *14*, 716.

(6) Amemori, S.; Sasaki, Y.; Yanai, N.; Kimizuka, N. Near-Infrared-to-Visible Photon Upconversion Sensitized by a Metal Complex with Spin-Forbidden yet Strong S_0-T_1 Absorption. *J. Am. Chem. Soc.* **2016**, *138*, 8702−8705.

(7) Sasaki, Y.; Yanai, N.; Kimizuka, N. Osmium Complex-Chromophore Conjugates with Both Singlet-to-Triplet Absorption and Long Triplet Lifetime through Tuning of the Heavy-Atom Effect. *Inorg. Chem.* **2021**, *61*, 5982−5990.

(8) Smitten, K. L.; Scattergood, P. A.; Kiker, C.; Thomas, J. A.; Elliott, P. I. P. Triazole-Based Osmium(II) Complexes Displaying Red/near-IR Luminescence: Antimicrobial Activity and Super-Resolution Imaging. *Chem. Sci.* **2020**, *11*, 8928−8935.

(9) Ravetz, B. D.; Tay, N. E. S.; Joe, C. L.; Sezen-Edmonds, M.; Schmidt, M. A.; Tan, Y.; Janey, J. M.; Eastgate, M. D.; Rovis, T. Development of a Platform for Near-Infrared Photoredox Catalysis. *ACS Cent. Sci.* **2020**, *6*, 2053−2059.

(10) Haruki, R.; Sasaki, Y.; Masutani, K.; Yanai, N.; Kimizuka, N. Leaping across the Visible Range: Near-Infrared-to-Violet Photon Upconversion Employing a Silyl-Substituted Anthracene. *Chem. Commun.* **2020**, *56*, 7017−7020.

(11) Favale, J. M.; Danilov, E. O.; Yarnell, J. E.; Castellano, F. N. Photophysical Processes in Rhenium(I) Diiminetricarbonyl Arylisocyanides Featuring Three Interacting Triplet Excited States. *Inorg. Chem.* **2019**, *58*, 8750−8762.

(12) Larsen, C. B.; Wenger, O. S. Photophysics and Photoredox Catalysis of a Homoleptic Rhenium(I) Tris(Diisocyanide) Complex. *Inorg. Chem.* **2018**, *57*, 2965−2968.

(13) Chakraborty, I.; Jimenez, J.; Sameera, W. M. C.; Kato, M.; Mascharak, P. K. Luminescent Re(I) Carbonyl Complexes as Trackable PhotoCORMs for CO Delivery to Cellular Targets. *Inorg. Chem.* **2017**, *56*, 2863−2873.

(14) Pierri, A. E.; Pallaoro, A.; Wu, G.; Ford, P. C. A Luminescent and Biocompatible PhotoCORM. *J. Am. Chem. Soc.* **2012**, *134*, 18197−18200.

(15) Xue, W. M.; Chan, M. C. W.; Su, Z. M.; Cheung, K. K.; Liu, S. T.; Che, C. M. Spectroscopic and Excited-State Properties of Luminescent Rhenium(I) N-Heterocyclic Carbene Complexes Containing Aromatic Diimine Ligands. *Organometallics* **1998**, *17*, 1622−1630.

(16) Lo, K. K. W. Luminescent Rhenium(I) and Iridium(III) Polypyridine Complexes as Biological Probes, Imaging Reagents, and Photocytotoxic Agents. *Acc. Chem. Res.* **2015**, *48*, 2985−2995.

(17) Chan, K. C.; Tong, K. M.; Cheng, S. C.; Ng, C. O.; Yiu, S. M.; Ko, C. C. Design of Luminescent Isocyano Rhenium(I) Complexes: Photophysics and Effects of the Ancillary Ligands. *Inorg. Chem.* **2018**, *57*, 13963−13972.

(18) Stout, M. J.; Skelton, B. W.; Sobolev, A. N.; Raiteri, P.; Massi, M.; Simpson, P. V. Synthesis and Photochemical Properties of Re(I) Tricarbonyl Complexes Bound to Thione and Thiazol-2-Ylidene Ligands. *Organometallics* **2020**, *39*, 3202−3211.

(19) Nicholls, T. P.; Burt, L. K.; Simpson, P. V.; Massi, M.; Bissember, A. C. Tricarbonyl Rhenium(I) Tetrazolato and N-Heterocyclic Carbene Complexes: Versatile Visible-Light-Mediated Photoredox Catalysts. *Dalton Trans.* **2019**, *48*, 12749−12754.

(20) Schmid, L.; Glaser, F.; Schaer, R.; Wenger, O. S. High Triplet Energy Iridium(III) Isocyanoborato Complex for Photochemical Upconversion, Photoredox and Energy Transfer Catalysis. *J. Am. Chem. Soc.* **2022**, *144*, 963−976.

(21) Diluzio, S.; Mdluli, V.; Connell, T. U.; Lewis, J.; Vanbenschoten, V.; Bernhard, S. High-Throughput Screening and Automated Data-Driven Analysis of the Triplet Photophysical Properties of Structurally Diverse, Heteroleptic Iridium(III) Complexes. *J. Am. Chem. Soc.* **2021**, *143*, 1179−1194.

(22) Coppo, P.; Plummer, E. A.; De Cola, L. Tuning Iridium(III) Phenylpyridine Complexes in the "Almost Blue" Region. *Chem. Commun.* **2004**, *4*, 1774−1775.

(23) Cañada, L. M.; Kölling, J.; Wen, Z.; Wu, J. I.; Teets, T. S. Cyano-Isocyanide Iridium(III) Complexes with Pure Blue Phosphorescence. *Inorg. Chem.* **2021**, *60*, 6391−6402.

(24) Pal, A. K.; Krotkus, S.; Fontani, M.; Mackenzie, C. F. R.; Cordes, D. B.; Slawin, A. M. Z.; Samuel, I. D. W.; Zysman-Colman, E. High-Efficiency Deep-Blue-Emitting Organic Light-Emitting Diodes Based on Iridium(III) Carbene Complexes. *Adv. Mater.* **2018**, *30*, 1−10.

(25) Bevernaegie, R.; Wehlin, S. A. M.; Piechota, E. J.; Abraham, M.; Philouze, C.; Meyer, G. J.; Elias, B.; Troian-Gautier, L. Improved Visible Light Absorption of Potent Iridium(III) Photo-Oxidants for Excited-State Electron Transfer Chemistry. *J. Am. Chem. Soc.* **2020**, *142*, 2732−2737.

(26) Shon, J. H.; Kim, D.; Rathnayake, M. D.; Sittel, S.; Weaver, J.; Teets, T. S. Photoredox Catalysis on Unactivated Substrates with Strongly Reducing Iridium Photosensitizers. *Chem. Sci.* **2021**, *12*, 4069−4078.

(27) Topics in Current Chemistry. In *Photochemistry and Photophysics of Coordination Compounds I*; Balzani, V.; Campagna, S., Eds.; Springer: Berlin Heidelberg: Berlin, Heidelberg, 2007; Vol. *280*.

(28) Topics in Current Chemistry. In *Photochemistry and Photophysics of Coordination Compounds II*; Balzani, V.; Campagna, S., Eds.; Springer: Berlin Heidelberg: Berlin, Heidelberg, 2007; Vol. *281*.

(29) Leis, W.; Argüello Cordero, M. A.; Lochbrunner, S.; Schubert, H.; Berkefeld, A. A Photoreactive Iron(II) Complex Luminophore. *J. Am. Chem. Soc.* **2022**, *144*, 1169−1173.

(30) Chábera, P.; Kjaer, K. S.; Prakash, O.; Honarfar, A.; Liu, Y.; Fredin, L. A.; Harlang, T. C. B.; Lidin, S.; Uhlig, J.; Sundström, V.; Lomoth, R.; Persson, P.; Wärnmark, K. Fe II Hexa N -Heterocyclic Carbene Complex with a 528 ps Metal-to-Ligand Charge-Transfer Excited-State Lifetime. *J. Phys. Chem. Lett.* **2018**, *9*, 459−463.

(31) Mengel, A. K. C. C.; Förster, C.; Breivogel, A.; Mack, K.; Ochsmann, J. R.; Laquai, F.; Ksenofontov, V.; Heinze, K. A Heteroleptic Push−Pull Substituted Iron(II) Bis(Tridentate) Com-

https://doi.org/10.1021/acs.inorgchem.2c01438
Inorg. Chem. 2022, 61, 10533−10547

plex with Low-Energy Charge-Transfer States. *Chem. – Eur. J.* **2015**, *21*, 704–714.
(32) Liu, Y.; Persson, P.; Sundström, V.; Wärnmark, K. Fe N-Heterocyclic Carbene Complexes as Promising Photosensitizers. *Acc. Chem. Res.* **2016**, *49*, 1477–1485.
(33) Liu, Y.; Harlang, T.; Canton, S. E.; Chábera, P.; Suárez-Alcántara, K.; Fleckhaus, A.; Vithanage, D. A.; Göransson, E.; Corani, A.; Lomoth, R.; Sundström, V.; Wärnmark, K. Towards Longer-Lived Metal-to-Ligand Charge Transfer States of Iron(II) Complexes: An N-Heterocyclic Carbene Approach. *Chem. Commun.* **2013**, *49*, 6412.
(34) Zimmer, P.; Burkhardt, L.; Friedrich, A.; Steube, J.; Neuba, A.; Schepper, R.; Müller, P.; Flörke, U.; Huber, M.; Lochbrunner, S.; Bauer, M. The Connection between NHC Ligand Count and Photophysical Properties in Fe(II) Photosensitizers: An Experimental Study. *Inorg. Chem.* **2018**, *57*, 360–373.
(35) Sarkar, B.; Suntrup, L. Illuminating Iron: Mesoionic Carbenes as Privileged Ligands in Photochemistry. *Angew. Chem., Int. Ed.* **2017**, *56*, 8938–8940.
(36) Dierks, P.; Vukadinovic, Y.; Bauer, M. Photoactive Iron Complexes: More Sustainable, but Still a Challenge. *Inorg. Chem. Front.* **2022**, *9*, 206–220.
(37) Vöhringer, P. Vibrations Tell the Tale. A Time-Resolved Mid-Infrared Perspective of the Photochemistry of Iron Complexes. *Dalton Trans.* **2020**, *49*, 256–266.
(38) Paulus, B. C.; Nielsen, K. C.; Tichnell, C. R.; Carey, M. C.; McCusker, J. K. A Modular Approach to Light Capture and Synthetic Tuning of the Excited-State Properties of Fe(II)-Based Chromophores. *J. Am. Chem. Soc.* **2021**, *143*, 8086–8098.
(39) Dierks, P.; Kruse, A.; Bokareva, O. S.; Al-Marri, M. J.; Kalmbach, J.; Baltrun, M.; Neuba, A.; Schoch, R.; Hohloch, S.; Heinze, K.; Seitz, M.; Kühn, O.; Lochbrunner, S.; Bauer, M. Distinct Photodynamics of κ-N and κ-C Pseudoisomeric Iron(II) Complexes. *Chem. Commun.* **2021**, *57*, 6640–6643.
(40) Paulus, B. C.; Adelman, S. L.; Jamula, L. L. L.; McCusker, J. K. K. Leveraging Excited-State Coherence for Synthetic Control of Ultrafast Dynamics. *Nature* **2020**, *582*, 214–218.
(41) Tang, Z.; Chang, X. Y.; Wan, Q.; Wang, J.; Ma, C.; Law, K. C.; Liu, Y.; Che, C. M. Bis(Tridentate) Iron(II) Complexes with a Cyclometalating Unit: Photophysical Property Enhancement with Combinatorial Strong Ligand Field Effect. *Organometallics* **2020**, *39*, 2791–2802.
(42) Braun, J. D.; Lozada, I. B.; Kolodziej, C.; Burda, C.; Newman, K. M. E.; van Lierop, J.; Davis, R. L.; Herbert, D. E. Iron(II) Coordination Complexes with Panchromatic Absorption and Nanosecond Charge-Transfer Excited State Lifetimes. *Nat. Chem.* **2019**, *11*, 1144–1150.
(43) Young, E. R.; Oldacre, A. Iron Hits the Mark. *Science.* **2019**, *363*, 225–226.
(44) Juban, E. A.; Smeigh, A. L.; Monat, J. E.; McCusker, J. K. Ultrafast Dynamics of Ligand-Field Excited States. *Coord. Chem. Rev.* **2006**, *250*, 1783–1791.
(45) Jamula, L. L.; Brown, A. M.; Guo, D.; McCusker, J. K. Synthesis and Characterization of a High-Symmetry Ferrous Polypyridyl Complex: Approaching the $^5T_2/^3T_1$ Crossing Point for Fe^{II}. *Inorg. Chem.* **2014**, *53*, 15–17.
(46) Treichel, P. M.; Dirreen, G. E. Electrochemical Oxidation of Isocyanide Complexes of Manganese and Chromium. *J. Organomet. Chem.* **1972**, *39*, C20–C22.
(47) Treichel, P. M.; Dirreen, G. E.; Mueh, H. J. Manganese(I) Isocyanide Complexes. *J. Organomet. Chem.* **1972**, *44*, 339–352.
(48) Treichel, P. M. Transition Metal-Lsocyanide Complexes. *Adv. Organomet. Chem.* **1973**, 21–86.
(49) Treichel, P. M.; Mueh, H. J. Synthesis and Electrochemistry of $C_5H_5Mn(CNR)_3$ Compounds. *Inorg. Chim. Acta* **1977**, *22*, 265–268.
(50) Treichel, P. M.; Mueh, H. J. Electrochemical Studies on $[Mn(CNR)_6]^+$ Complexes. *Inorg. Chem.* **1977**, *16*, 1167–1169.
(51) Treichel, P. M.; Firsich, D. W.; Essenmacher, G. P. Manganese(I) and Chromium(0) Complexes of Phenyl Isocyanide. *Inorg. Chem.* **1979**, *18*, 2405–2409.
(52) Treichel, P. M. Manganese. In *Comprehensive Organometallic Chemistry*; Elsevier, 1982; Vol. *4*, pp 1–159.
(53) Mann, K. R.; Cimolino, M.; Geoffroy, G. L.; Hammond, G. S.; Orio, A. A.; Albertin, G.; Gray, H. B. Electronic Structures and Spectra of Hexakisphenylisocyanide Complexes of Cr(0), Mo(0), W(0), Mn(I), and Mn(II). *Inorg. Chim. Acta* **1976**, *16*, 97–101.
(54) Herr, P.; Kerzig, C.; Larsen, C. B.; Häussinger, D.; Wenger, O. S. Manganese(I) Complexes with Metal-to-Ligand Charge Transfer Luminescence and Photoreactivity. *Nat. Chem.* **2021**, *13*, 956–962.
(55) Büldt, L. A.; Wenger, O. S. Chromium(0), Molybdenum(0), and Tungsten(0) Isocyanide Complexes as Luminophores and Photosensitizers with Long-Lived Excited States. *Angew. Chem., Int. Ed.* **2017**, *56*, 5676–5682.
(56) Melcher, F.; Wilken, H. Die Verfügbarkeit von Hochtechnologie-Rohstoffen. *Chem. Unserer Zeit* **2013**, *47*, 32–49.
(57) Wegeberg, C.; Wenger, O. S. Luminescent First-Row Transition Metal Complexes. *JACS Au* **2021**, *1*, 1860–1876.
(58) Förster, C.; Heinze, K. Photophysics and Photochemistry with Earth-Abundant Metals-Fundamentals and Concepts. *Chem. Soc. Rev.* **2020**, *49*, 1057–1070.
(59) Wenger, O. S. Photoactive Complexes with Earth-Abundant Metals. *J. Am. Chem. Soc.* **2018**, *140*, 13522–13533.
(60) McCusker, J. K. Electronic Structure in the Transition Metal Block and Its Implications for Light Harvesting. *Science.* **2019**, *363*, 484–488.
(61) Zobel, J. P.; González, L. The Quest to Simulate Excited-State Dynamics of Transition Metal Complexes. *JACS Au* **2021**, *1*, 1116–1140.
(62) Dorn, M.; Kalmbach, J.; Boden, P.; Päpcke, A.; Gómez, S.; Förster, C.; Kuczelinis, F.; Carrella, L. M.; Büldt, L. A.; Bings, N. H.; Rentschler, E.; Lochbrunner, S.; González, L.; Gerhards, M.; Seitz, M.; Heinze, K. A Vanadium(III) Complex with Blue and NIR-II Spin-Flip Luminescence in Solution. *J. Am. Chem. Soc.* **2020**, *142*, 7947–7955.
(63) Dorn, M.; Kalmbach, J.; Boden, P.; Kruse, A.; Dab, C.; Reber, C.; Niedner-Schatteburg, G.; Lochbrunner, S.; Gerhards, M.; Seitz, M.; Heinze, K. Ultrafast and Long-Time Excited State Kinetics of an NIR-Emissive Vanadium(III) Complex I: Synthesis, Spectroscopy and Static Quantum Chemistry. *Chem. Sci.* **2021**, *12*, 10780–10790.
(64) Fataftah, M. S.; Bayliss, S. L.; Laorenza, D. W.; Wang, X.; Phelan, B. T.; Wilson, C. B.; Mintun, P. J.; Kovos, B. D.; Wasielewski, M. R.; Han, S.; Sherwin, M. S.; Awschalom, D. D.; Freedman, D. E. Trigonal Bipyramidal V^{3+} Complex as an Optically Addressable Molecular Qubit Candidate. *J. Am. Chem. Soc.* **2020**, *142*, 20400–20408.
(65) Zobel, J. P.; Knoll, T.; González, L. Ultrafast and Long-Time Excited State Kinetics of an NIR-Emissive Vanadium(III) Complex II. Elucidating Triplet-to-Singlet Excited-State Dynamics. *Chem. Sci.* **2021**, *12*, 10791–10801.
(66) Büldt, L. A.; Guo, X.; Vogel, R.; Prescimone, A.; Wenger, O. S. A Tris(Diisocyanide)Chromium(0) Complex is a Luminescent Analog of $Fe(2,2'\text{-Bipyridine})_3^{2+}$. *J. Am. Chem. Soc.* **2017**, *139*, 985–992.
(67) Wegeberg, C.; Häussinger, D.; Wenger, O. S. Pyrene-Decoration of a Chromium(0) Tris(Diisocyanide) Enhances Excited State Delocalization: A Strategy to Improve the Photoluminescence of $3d^6$ Metal Complexes. *J. Am. Chem. Soc.* **2021**, *143*, 15800–15811.
(68) Sinha, N.; Jiménez, J.-R.; Pfund, B.; Prescimone, A.; Piguet, C.; Wenger, O. S. A Near-Infrared-II Emissive Chromium(III) Complex. *Angew. Chem., Int. Ed.* **2021**, *60*, 23722–23728.
(69) Wang, C.; Otto, S.; Dorn, M.; Kreidt, E.; Lebon, J.; Sršan, L.; Di Martino-Fumo, P.; Gerhards, M.; Resch-Genger, U.; Seitz, M.; Heinze, K. Deuterated Molecular Ruby with Record Luminescence Quantum Yield. *Angew. Chem., Int. Ed.* **2018**, *57*, 1112–1116.
(70) Jiménez, J.-R.; Doistau, B.; Cruz, C. M.; Besnard, C.; Cuerva, J. M.; Campaña, A. G.; Piguet, C. Chiral Molecular Ruby $[Cr(dqp)_2]^{3+}$ with Long-Lived Circularly Polarized Luminescence. *J. Am. Chem. Soc.* **2019**, *141*, 13244–13252.

https://doi.org/10.1021/acs.inorgchem.2c01438
Inorg. Chem. 2022, 61, 10533–10547

(71) Jiménez, J.; Poncet, M.; Míguez-Lago, S.; Grass, S.; Lacour, J.; Besnard, C.; Cuerva, J. M.; Campaña, A. G.; Piguet, C. Bright Long-Lived Circularly Polarized Luminescence in Chiral Chromium(III) Complexes. *Angew. Chem., Int. Ed.* **2021**, *60*, 10095−10102.
(72) Conti, C.; Castelli, F.; Forster, L. S. Photophysics of Hexakis(Cyano)Chromate(3-) and Hexakis(Cyano)Cobaltate(3-) in Polyalcohol-Water Solutions at Room Temperature. *J. Phys. Chem. A* **1979**, *83*, 2371−2376.
(73) Reichenauer, F.; Wang, C.; Förster, C.; Boden, P.; Ugur, N.; Báez-Cruz, R.; Kalmbach, J.; Carrella, L. M.; Rentschler, E.; Ramanan, C.; Niedner-Schatteburg, G.; Gerhards, M.; Seitz, M.; Resch-Genger, U.; Heinze, K. Strongly Red-Emissive Molecular Ruby $[Cr(bpmp)_2]^{3+}$ Surpasses $[Ru(bpy)_3]^{2+}$. *J. Am. Chem. Soc.* **2021**, *143*, 11843−11855.
(74) Farran, R.; Le-Quang, L.; Mouesca, J. M.; Maurel, V.; Jouvenot, D.; Loiseau, F.; Deronzier, A.; Chauvin, J. $[Cr(ttpy)_2]^{3+}$ as a Multi-Electron Reservoir for Photoinduced Charge Accumulation. *Dalton Trans.* **2019**, *48*, 6800−6811.
(75) Qin, Y.; She, P.; Huang, X.; Huang, W.; Zhao, Q. Luminescent Manganese(II) Complexes: Synthesis, Properties and Optoelectronic Applications. *Coord. Chem. Rev.* **2020**, *416*, No. 213331.
(76) Jimenez, J.; Chakraborty, I.; Dominguez, A.; Martinez-Gonzalez, J.; Sameera, W. M. C.; Mascharak, P. K. A Luminescent Manganese PhotoCORM for CO Delivery to Cellular Targets under the Control of Visible Light. *Inorg. Chem.* **2018**, *57*, 1766−1773.
(77) Harris, J. P.; Reber, C.; Colmer, H. E.; Jackson, T. A.; Forshaw, A. P.; Smith, J. M.; Kinney, R. A.; Telser, J. Near-Infrared $^2E_g \rightarrow {}^4A_{2g}$ and Visible LMCT Luminescence from a Molecular Bis-(Tris-(Carbene)Borate) Manganese(IV) Complex. *Can. J. Chem.* **2017**, *95*, 547−552.
(78) Chábera, P.; Liu, Y.; Prakash, O.; Thyrhaug, E.; El Nahhas, A.; Honarfar, A.; Essén, S.; Fredin, L. A.; Harlang, T. C. B.; Kjær, K. S.; Handrup, K.; Ericson, F.; Tatsuno, H.; Morgan, K.; Schnadt, J.; Häggström, L.; Ericsson, T.; Sobkowiak, A.; Lidin, S.; Huang, P.; Styring, S.; Uhlig, J.; Bendix, J.; Lomoth, R.; Sundström, V.; Persson, P.; Wärnmark, K. A Low-Spin Fe(III) Complex with 100-ps Ligand-to-Metal Charge Transfer Photoluminescence. *Nature* **2017**, *543*, 695−699.
(79) Kjær, K. S.; Kaul, N.; Prakash, O.; Chábera, P.; Rosemann, N. W.; Honarfar, A.; Gordivska, O.; Fredin, L. A.; Bergquist, K.-E. E.; Häggström, L.; Ericsson, T.; Lindh, L.; Yartsev, A.; Styring, S.; Huang, P.; Uhlig, J.; Bendix, J.; Strand, D.; Sundström, V.; Persson, P.; Lomoth, R.; Wärnmark, K. Luminescence and Reactivity of a Charge-Transfer Excited Iron Complex with Nanosecond Lifetime. *Science* **2019**, *363*, 249−253.
(80) Lindh, L.; Chábera, P.; Rosemann, N. W.; Uhlig, J.; Wärnmark, K.; Yartsev, A.; Sundström, V.; Persson, P. Photophysics and Photochemistry of Iron Carbene Complexes for Solar Energy Conversion and Photocatalysis. *Catalysts* **2020**, *10*, No. 315.
(81) Pal, A. K.; Li, C.; Hanan, G. S.; Zysman-Colman, E. Blue-Emissive Cobalt(III) Complexes and Their Use in the Photocatalytic Trifluoromethylation of Polycyclic Aromatic Hydrocarbons. *Angew. Chem.* **2018**, *130*, 8159−8163.
(82) Kaufhold, S.; Rosemann, N. W.; Chábera, P.; Lindh, L.; Bolaño Losada, I.; Uhlig, J.; Pascher, T.; Strand, D.; Wärnmark, K.; Yartsev, A.; Persson, P. Microsecond Photoluminescence and Photoreactivity of a Metal-Centered Excited State in a Hexacarbene-Co(III) Complex. *J. Am. Chem. Soc.* **2021**, *143*, 1307−1312.
(83) Viaene, L.; D'Olieslager, J. Luminescence from and Absorption by the $^3T_{1g}$ Level of the Hexacyanocobaltate(III) Ion. *Inorg. Chem.* **1987**, *26*, 960−962.
(84) Sinha, N.; Pfund, B.; Wegeberg, C.; Prescimone, A.; Wenger, O. S. Cobalt Carbene(III) Complex with an Electronic Excited State Structure Similar to Cyclometalated Iridium(III) Compounds. *J. Am. Chem. Soc.* **2022**, *144*, 9859−9873.
(85) Malzkuhn, S.; Wenger, O. S. Luminescent Ni(0) Complexes. *Coord. Chem. Rev.* **2018**, *359*, 52−56.
(86) Büldt, L. A.; Larsen, C. B.; Wenger, O. S. Luminescent Ni^0 Diisocyanide Chelates as Analogues of Cu^I Diimine Complexes. *Chem. - Eur. J.* **2017**, *23*, 8577−8580.
(87) Wong, Y. S.; Tang, M. C.; Ng, M.; Yam, V. W. W. Toward the Design of Phosphorescent Emitters of Cyclometalated Earth-Abundant Nickel(II) and Their Supramolecular Study. *J. Am. Chem. Soc.* **2020**, *142*, 7638−7646.
(88) Cope, J. D.; Denny, J. A.; Lamb, R. W.; McNamara, L. E.; Hammer, N. I.; Webster, C. E.; Hollis, T. K. Synthesis, Characterization, Photophysics, and a Ligand Rearrangement of CCC-NHC Pincer Nickel Complexes: Colors, Polymorphs, Emission, and Raman Spectra. *J. Organomet. Chem.* **2017**, *845*, 258−265.
(89) Hamze, R.; Peltier, J. L.; Sylvinson, D.; Jung, M.; Cardenas, J.; Haiges, R.; Soleilhavoup, M.; Jazzar, R.; Djurovich, P. I.; Bertrand, G.; Thompson, M. E. Eliminating Nonradiative Decay in Cu(I) Emitters:>99% Quantum Efficiency and Microsecond Lifetime. *Science* **2019**, *363*, 601−606.
(90) Lazorski, M. S.; Castellano, F. N. Advances in the Light Conversion Properties of Cu(I)-Based Photosensitizers. *Polyhedron* **2014**, *82*, 57−70.
(91) Shi, S.; Jung, M. C.; Coburn, C.; Tadle, A.; Sylvinson, D. M. R.; Djurovich, P. I.; Forrest, S. R.; Thompson, M. E. Highly Efficient Photo- and Electroluminescence from Two-Coordinate Cu(I) Complexes Featuring Nonconventional N-Heterocyclic Carbenes. *J. Am. Chem. Soc.* **2019**, *141*, 3576−3588.
(92) Nicholls, T. P.; Bissember, A. C. Developments in Visible-Light-Mediated Copper Photocatalysis. *Tetrahedron Lett.* **2019**, *60*, No. 150883.
(93) Rentschler, M.; Schmid, M. A.; Frey, W.; Tschierlei, S.; Karnahl, M. Multidentate Phenanthroline Ligands Containing Additional Donor Moieties and Their Resulting Cu(I) and Ru(II) Photosensitizers: A Comparative Study. *Inorg. Chem.* **2020**, *59*, 14762−14771.
(94) Housecroft, C. E.; Constable, E. C. The Emergence of Copper(I)-Based Dye Sensitized Solar Cells. *Chem. Soc. Rev.* **2015**, *44*, 8386−8398.
(95) Gernert, M.; Balles-Wolf, L.; Kerner, F.; Müller, U.; Schmiedel, A.; Holzapfel, M.; Marian, C. M.; Pflaum, J.; Lambert, C.; Steffen, A. Cyclic (Amino)(Aryl)Carbenes Enter the Field of Chromophore Ligands: Expanded π System Leads to Unusually Deep Red Emitting Cu^I Compounds. *J. Am. Chem. Soc.* **2020**, *142*, 8897−8909.
(96) Hölzel, T.; Belyaev, A.; Terzi, M.; Stenzel, L.; Gernert, M.; Marian, C. M.; Steffen, A.; Ganter, C. Linear Carbene Pyridine Copper Complexes with Sterically Demanding N, N′-Bis(Trityl)-Imidazolylidene: Syntheses, Molecular Structures, and Photophysical Properties. *Inorg. Chem.* **2021**, *60*, 18529−18543.
(97) Schinabeck, A.; Chen, J.; Kang, L.; Teng, T.; Homeier, H. H. H.; Suleymanova, A. F.; Shafikov, M. Z.; Yu, R.; Lu, C. Z.; Yersin, H. Symmetry-Based Design Strategy for Unprecedentedly Fast Decaying Thermally Activated Delayed Fluorescence (TADF). Application to Dinuclear Cu(I) Compounds. *Chem. Mater.* **2019**, *31*, 4392−4404.
(98) Hofbeck, T.; Monkowius, U.; Yersin, H. Highly Efficient Luminescence of Cu(I) Compounds: Thermally Activated Delayed Fluorescence Combined with Short-Lived Phosphorescence. *J. Am. Chem. Soc.* **2015**, *137*, 399−404.
(99) Wegeberg, C.; Wenger, O. S. Luminescent Chromium(0) and Manganese(I) Complexes. *Dalton Trans.* **2022**, *51*, 1297−1302.
(100) Larsen, C. B.; Wenger, O. S. Photoredox Catalysis with Metal Complexes Made from Earth-Abundant Elements. *Chem. - Eur. J.* **2018**, *24*, 2039−2058.
(101) Mann, K. R.; Gray, H. B.; Hammond, G. S. Excited-State Reactivity Patterns of Hexakisarylisocyano Complexes of Chromium(0), Molybdenum(0), and Tungsten(0). *J. Am. Chem. Soc.* **1977**, *99*, 306−307.
(102) Sattler, W.; Ener, M. E.; Blakemore, J. D.; Rachford, A. A.; LaBeaume, P. J.; Thackeray, J. W.; Cameron, J. F.; Winkler, J. R.; Gray, H. B. Generation of Powerful Tungsten Reductants by Visible Light Excitation. *J. Am. Chem. Soc.* **2013**, *135*, 10614−10617.
(103) Sattler, W.; Henling, L. M.; Winkler, J. R.; Gray, H. B. Bespoke Photoreductants: Tungsten Arylisocyanides. *J. Am. Chem. Soc.* **2015**, *137*, 1198−1205.

https://doi.org/10.1021/acs.inorgchem.2c01438
Inorg. Chem. 2022, 61, 10533−10547

(104) Kvapilová, H.; Sattler, W.; Sattler, A.; Sazanovich, I. V.; Clark, I. P.; Towrie, M.; Gray, H. B.; Záliš, S.; Vlček, A. Electronic Excited States of Tungsten(0) Arylisocyanides. *Inorg. Chem.* **2015**, *54*, 8518−8528.
(105) Takematsu, K.; Wehlin, S. A. M.; Sattler, W.; Winkler, J. R.; Gray, H. B. Two-Photon Spectroscopy of Tungsten(0) Arylisocyanides Using Nanosecond-Pulsed Excitation. *Dalton Trans.* **2017**, *46*, 13188−13193.
(106) Fajardo, J.; Schwan, J.; Kramer, W. W.; Takase, M. K.; Winkler, J. R.; Gray, H. B. Third-Generation $W(CNAr)_6$ Photoreductants (CNAr = Fused-Ring and Alkynyl-Bridged Arylisocyanides). *Inorg. Chem.* **2021**, *60*, 3481−3491.
(107) Fajardo, J.; Barth, A. T.; Morales, M.; Takase, M. K.; Winkler, J. R.; Gray, H. B. Photoredox Catalysis Mediated by Tungsten(0) Arylisocyanides. *J. Am. Chem. Soc.* **2021**, *143*, 19389−19398.
(108) Monat, J. E.; McCusker, J. K. Femtosecond Excited-State Dynamics of an Iron(II) Polypyridyl Solar Cell Sensitizer Model. *J. Am. Chem. Soc.* **2000**, *122*, 4092−4097.
(109) Cannizzo, A.; Milne, C. J.; Consani, C.; Gawelda, W.; Bressler, C.; van Mourik, F.; Chergui, M. Light-Induced Spin Crossover in Fe(II)-Based Complexes: The Full Photocycle Unraveled by Ultrafast Optical and X-Ray Spectroscopies. *Coord. Chem. Rev.* **2010**, *254*, 2677−2686.
(110) Zhang, W.; Alonso-Mori, R.; Bergmann, U.; Bressler, C.; Chollet, M.; Galler, A.; Gawelda, W.; Hadt, R. G.; Hartsock, R. W.; Kroll, T.; Kjær, K. S.; Kubiek, K.; Lemke, H. T.; Liang, H. W.; Meyer, D. A.; Nielsen, M. M.; Purser, C.; Robinson, J. S.; Solomon, E. I.; Sun, Z.; Sokaras, D.; Van Driel, T. B.; Vankó, G.; Weng, T. C.; Zhu, D.; Gaffney, K. J. Tracking Excited-State Charge and Spin Dynamics in Iron Coordination Complexes. *Nature* **2014**, *509*, 345−348.
(111) Harlang, T. C. B.; Liu, Y.; Gordivska, O.; Fredin, L. A.; Ponseca, C. S.; Huang, P.; Chábera, P.; Kjaer, K. S.; Mateos, H.; Uhlig, J.; Lomoth, R.; Wallenberg, R.; Styring, S.; Persson, P.; Sundström, V.; Wärnmark, K. Iron Sensitizer Converts Light to Electrons with 92% Yield. *Nat. Chem.* **2015**, *7*, 883−889.
(112) Duchanois, T.; Etienne, T.; Cebrián, C.; Liu, L.; Monari, A.; Beley, M.; Assfeld, X.; Haacke, S.; Gros, P. C. An Iron-Based Photosensitizer with Extended Excited-State Lifetime: Photophysical and Photovoltaic Properties. *Eur. J. Inorg. Chem.* **2015**, *2015*, 2469−2477.
(113) Zhang, W.; Kjær, K. S.; Alonso-Mori, R.; Bergmann, U.; Chollet, M.; Fredin, L. A.; Hadt, R. G.; Hartsock, R. W.; Harlang, T.; Kroll, T.; Kubiček, K.; Lemke, H. T.; Liang, H. W.; Liu, Y.; Nielsen, M. M.; Persson, P.; Robinson, J. S.; Solomon, E. I.; Sun, Z.; Sokaras, D.; van Driel, T. B.; Weng, T.-C.; Zhu, D.; Wärnmark, K.; Sundström, V.; Gaffney, K. J. Manipulating Charge Transfer Excited State Relaxation and Spin Crossover in Iron Coordination Complexes with Ligand Substitution. *Chem. Sci.* **2017**, *8*, 515−523.
(114) Chen, J.; Browne, W. R. Photochemistry of Iron Complexes. *Coord. Chem. Rev.* **2018**, *374*, 15−35.
(115) Zhang, K.; Ash, R.; Girolami, G. S.; Vura-Weis, J. Tracking the Metal-Centered Triplet in Photoinduced Spin Crossover of $Fe(phen)_3^{2+}$ with Tabletop Femtosecond M-Edge X-Ray Absorption Near-Edge Structure Spectroscopy. *J. Am. Chem. Soc.* **2019**, *141*, 17180−17188.
(116) Francés-Monerris, A.; Gros, P. C.; Assfeld, X.; Monari, A.; Pastore, M. Toward Luminescent Iron Complexes: Unravelling the Photophysics by Computing Potential Energy Surfaces. *ChemPhotoChem* **2019**, *3*, 666−683.
(117) Benaicha, B.; Van Do, K.; Yangui, A.; Pittala, N.; Lusson, A.; Sy, M.; Bouchez, G.; Fourati, H.; Gómez-Garciá, C. J.; Triki, S.; Boukheddaden, K. Interplay between Spin-Crossover and Luminescence in a Multifunctional Single Crystal Iron(II) Complex: Towards a New Generation of Molecular Sensors. *Chem. Sci.* **2019**, *10*, 6791−6798.
(118) Kjær, K. S.; Van Driel, T. B.; Harlang, T. C. B.; Kunnus, K.; Biasin, E.; Ledbetter, K.; Hartsock, R. W.; Reinhard, M. E.; Koroidov, S.; Li, L.; Laursen, M. G.; Hansen, F. B.; Vester, P.; Christensen, M.; Haldrup, K.; Nielsen, M. M.; Dohn, A. O.; Pápai, M. I.; Møller, K. B.; Chabera, P.; Liu, Y.; Tatsuno, H.; Timm, C.; Jarenmark, M.; Uhlig, J.; Sundstöm, V.; Wärnmark, K.; Persson, P.; Németh, Z.; Szemes, D. S.; Bajnóczi, É.; Vankó, G.; Alonso-Mori, R.; Glownia, J. M.; Nelson, S.; Sikorski, M.; Sokaras, D.; Canton, S. E.; Lemke, H. T.; Gaffney, K. J. Finding Intersections between Electronic Excited State Potential Energy Surfaces with Simultaneous Ultrafast X-Ray Scattering and Spectroscopy. *Chem. Sci.* **2019**, *10*, 5749−5760.
(119) Kottelat, E.; Zobi, F. Visible Light-Activated PhotoCORMs. *Inorganics* **2017**, *5*, No. 24.
(120) Ji, X.; Damera, K.; Zheng, Y.; Yu, B.; Otterbein, L. E.; Wang, B. Toward Carbon Monoxide-Based Therapeutics: Critical Drug Delivery and Developability Issues. *J. Pharm. Sci.* **2016**, *105*, 406−416.
(121) Kottelat, E.; Ruggi, A.; Zobi, F. Red-Light Activated PhotoCORMs of Mn(I) Species Bearing Electron Deficient 2,2′-Azopyridines. *Dalton Trans.* **2016**, *45*, 6920−6927.
(122) Stout, M. J.; Stefan, A.; Skelton, B. W.; Sobolev, A. N.; Massi, M.; Hochkoeppler, A.; Stagni, S.; Simpson, P. V. Synthesis and Photochemical Properties of Manganese(I) Tricarbonyl Diimine Complexes Bound to Tetrazolato Ligands. *Eur. J. Inorg. Chem.* **2020**, *2020*, 292−298.
(123) Tang, M.; Cameron, L.; Poland, E. M.; Yu, L.-J.; Moggach, S. A.; Fuller, R. O.; Huang, H.; Sun, J.; Thickett, S. C.; Massi, M.; Coote, M. L.; Ho, C. C.; Bissember, A. C. Photoactive Metal Carbonyl Complexes Bearing N-Heterocyclic Carbene Ligands: Synthesis, Characterization, and Viability as Photoredox Catalysts. *Inorg. Chem.* **2022**, *61*, 1888−1898.
(124) Cole-Filipiak, N. C.; Troß, J.; Schrader, P.; McCaslin, L. M.; Ramasesha, K. Ultrafast Infrared Transient Absorption Spectroscopy of Gas-Phase $Ni(CO)_4$ Photodissociation at 261 Nm. *J. Chem. Phys.* **2022**, *156*, No. 144306.
(125) Marhenke, J.; Trevino, K.; Works, C. The Chemistry, Biology and Design of Photochemical CO Releasing Molecules and the Efforts to Detect CO for Biological Applications. *Coord. Chem. Rev.* **2016**, *306*, 533−543.
(126) Schatzschneider, U. PhotoCORMs: Light-Triggered Release of Carbon Monoxide from the Coordination Sphere of Transition Metal Complexes for Biological Applications. *Inorg. Chim. Acta* **2011**, *374*, 19−23.
(127) Chakraborty, I.; Carrington, S. J.; Mascharak, P. K. Design Strategies to Improve the Sensitivity of Photoactive Metal Carbonyl Complexes (PhotoCORMs) to Visible Light and Their Potential as CO-Donors to Biological Targets. *Acc. Chem. Res.* **2014**, *47*, 2603−2611.
(128) Rimmer, R. D.; Pierri, A. E.; Ford, P. C. Photochemically Activated Carbon Monoxide Release for Biological Targets. Toward Developing Air-Stable PhotoCORMs Labilized by Visible Light. *Coord. Chem. Rev.* **2012**, *256*, 1509−1519.
(129) Rudolf, P.; Kanal, F.; Knorr, J.; Nagel, C.; Niesel, J.; Brixner, T.; Schatzschneider, U.; Nuernberger, P. Ultrafast Photochemistry of a Manganese-Tricarbonyl CO-Releasing Molecule (CORM) in Aqueous Solution. *J. Phys. Chem. Lett.* **2013**, *4*, 596−602.
(130) Heinemann, S. H.; Hoshi, T.; Westerhausen, M.; Schiller, A. Carbon Monoxide − Physiology, Detection and Controlled Release. *Chem. Commun.* **2014**, *50*, 3644−3660.
(131) Schatzschneider, U. Novel Lead Structures and Activation Mechanisms for CO-Releasing Molecules (CORMs). *Br. J. Pharmacol.* **2015**, *172*, 1638−1650.
(132) Wright, M. A.; Wright, J. A. PhotoCORMs: CO Release Moves into the Visible. *Dalton Trans.* **2016**, *45*, 6801−6811.
(133) Gottlieb, H. E.; Kotlyar, V.; Nudelman, A. NMR Chemical Shifts of Common Laboratory Solvents as Trace Impurities. *J. Org. Chem.* **1997**, *3263*, 7512−7515.
(134) Fulmer, G. R.; Miller, A. J. M.; Sherden, N. H.; Gottlieb, H. E.; Nudelman, A.; Stoltz, B. M.; Bercaw, J. E.; Goldberg, K. I. NMR Chemical Shifts of Trace Impurities: Common Laboratory Solvents, Organics, and Gases in Deuterated Solvents Relevant to the Organometallic Chemist. *Organometallics* **2010**, *29*, 2176−2179.
(135) Babij, N. R.; McCusker, E. O.; Whiteker, G. T.; Canturk, B.; Choy, N.; Creemer, L. C.; Amicis, C. V. D.; Hewlett, N. M.; Johnson,

P. L.; Knobelsdorf, J. A.; Li, F.; Lorsbach, B. A.; Nugent, B. M.; Ryan, S. J.; Smith, M. R.; Yang, Q. NMR Chemical Shifts of Trace Impurities: Industrially Preferred Solvents Used in Process and Green Chemistry. *Org. Process Res. Dev.* **2016**, *20*, 661−667.
(136) Harris, R. K.; Becker, E. D.; Cabral de Menezes, S. M.; Goodfellow, R.; Granger, P. NMR Nomenclature. Nuclear Spin Properties and Conventions for Chemical Shifts (IUPAC Recommendations 2001). *Pure Appl. Chem.* **2001**, *73*, 1795−1818.
(137) Aranzaes, J. R.; Daniel, M.-C.; Astruc, D. Metallocenes as References for the Determination of Redox Potentials by Cyclic Voltammetry - Permethylated Iron and Cobalt Sandwich Complexes, Inhibition by Polyamine Dendrimers, and the Role of Hydroxy-Containing Ferrocenes. *Can. J. Chem.* **2006**, *84*, 288−299.
(138) Bourhis, L. J.; Dolomanov, O. V.; Gildea, R. J.; Howard, J. A. K.; Puschmann, H. The Anatomy of a Comprehensive Constrained, Restrained Refinement Program for the Modern Computing Environment - Olex2 Dissected. *Acta Crystallogr., Sect. A: Found. Crystallogr.* **2015**, *71*, 59−75.
(139) Dolomanov, O. V.; Bourhis, L. J.; Gildea, R. J.; Howard, J. A. K.; Puschmann, H. OLEX2: A Complete Structure Solution, Refinement and Analysis Program. *J. Appl. Crystallogr.* **2009**, *42*, 339−341.
(140) Sheldrick, G. M. Crystal Structure Refinement with SHELXL. *Acta Crystallogr., Sect. C: Struct. Chem.* **2015**, *71*, 3−8.
(141) Macrae, C. F.; Edgington, P. R.; McCabe, P.; Pidcock, E.; Shields, G. P.; Taylor, R.; Towler, M.; van de Streek, J. Mercury: Visualization and Analysis of Crystal Structures. *J. Appl. Crystallogr.* **2006**, *39*, 453−457.
(142) Macrae, C. F.; Bruno, I. J.; Chisholm, J. A.; Edgington, P. R.; McCabe, P.; Pidcock, E.; Rodriguez-Monge, L.; Taylor, R.; van de Streek, J.; Wood, P. A. Mercury CSD 2.0 - New Features for the Visualization and Investigation of Crystal Structures. *J. Appl. Crystallogr.* **2008**, *41*, 466−470.
(143) CYL; Legault, C. Y. Université de Sherbrooke, 2020 (https://www.cylview.org).
(144) Allen, F. H. The Cambridge Structural Database: A Quarter of a Million Crystal Structures and Rising. *Acta Crystallogr., Sect. B: Struct. Sci.* **2002**, *58*, 380−388.
(145) Groom, C. R.; Allen, F. H. The Cambridge Structural Database in Retrospect and Prospect. *Angew. Chem., Int. Ed.* **2014**, *53*, 662−671.
(146) Groom, C. R.; Bruno, I. J.; Lightfoot, M. P.; Ward, S. C. The Cambridge Structural Database. *Acta Crystallogr., Sect. B: Struct. Sci., Cryst. Eng. Mater.* **2016**, *72*, 171−179.
(147) Neese, F. The ORCA Program System. *Wiley Interdiscip. Rev.: Comput. Mol. Sci.* **2012**, *2*, 73−78.
(148) Neese, F. Software Update: The ORCA Program System, Version 4.0. *Wiley Interdiscip. Rev.: Comput. Mol. Sci.* **2018**, *8*, No. e1327.
(149) Neese, F.; Wennmohs, F.; Becker, U.; Riplinger, C. The ORCA Quantum Chemistry Program Package. *J. Chem. Phys.* **2020**, *152*, No. 224108.
(150) Grimme, S.; Brandenburg, J. G.; Bannwarth, C.; Hansen, A. Consistent Structures and Interactions by Density Functional Theory with Small Atomic Orbital Basis Sets. *J. Chem. Phys.* **2015**, *143*, No. 054107.
(151) Brandenburg, J. G.; Bannwarth, C.; Hansen, A.; Grimme, S. B97-3c: A Revised Low-Cost Variant of the B97-D Density Functional Method. *J. Chem. Phys.* **2018**, *148*, No. 064104.
(152) Grimme, S.; Antony, J.; Ehrlich, S.; Krieg, H. A Consistent and Accurate Ab Initio Parametrization of Density Functional Dispersion Correction (DFT-D) for the 94 Elements H-Pu. *J. Chem. Phys.* **2010**, *132*, No. 154104.
(153) Grimme, S.; Ehrlich, S.; Goerigk, L. Effect of the Damping Function in Dispersion Corrected Density Functional Theory. *J. Comput. Chem.* **2011**, *32*, 1456−1465.
(154) Kruse, H.; Grimme, S. A Geometrical Correction for the Inter- and Intra-Molecular Basis Set Superposition Error in Hartree-Fock and Density Functional Theory Calculations for Large Systems. *J. Chem. Phys.* **2012**, *136*, No. 154101.
(155) Weigend, F. Accurate Coulomb-Fitting Basis Sets for H to Rn. *Phys. Chem. Chem. Phys.* **2006**, *8*, 1057−1065.
(156) Libint; Valeev, E. F. http://libint.valeyev.net.
(157) Chemcraft - Graphical Software for Visualization of Quantum Chemistry Computations.
(158) Bilger, J. B.; Kerzig, C.; Larsen, C. B.; Wenger, O. S. A Photorobust Mo(0) Complex Mimicking $[Os(2,2'\text{-bipyridine})_3]^{2+}$ and Its Application in Red-to-Blue Upconversion. *J. Am. Chem. Soc.* **2021**, *143*, 1651−1663.
(159) Patil, P.; Ahmadian-Moghaddam, M.; Dömling, A. Isocyanide 2.0. *Green Chem.* **2020**, *22*, 6902−6911.
(160) Nielson, R. M.; Wherland, S. Multinuclear NMR Studies of $Mn(CNR)_6^{+,2+}$: R = Methyl, Ethyl, Isopropyl, Tert-Butyl, Cyclohexyl, Benzyl, Phenyl, p-Tolyl, and p-Anisyl. *Inorg. Chem.* **1985**, *24*, 3458−3464.
(161) Iasco, O.; Boillot, M.-L.; Bellec, A.; Guillot, R.; Rivière, E.; Mazerat, S.; Nowak, S.; Morineau, D.; Brosseau, A.; Miserque, F.; Repain, V.; Mallah, T. The Disentangling of Hysteretic Spin Transition, Polymorphism and Metastability in Bistable Thin Films Formed by Sublimation of Bis(Scorpionate) Fe(II) Molecules. *J. Mater. Chem. C* **2017**, *5*, 11067−11075.
(162) Guionneau, P.; Marchivie, M.; Bravic, G.; Létard, J.-F.; Chasseau, D. Structural Aspects of Spin Crossover. Example of the $[Fe^{II}L_n(NCS)_2]$ Complexes. In *Spin Crossover in Transition Metal Compounds II; Topics in Current Chemistry*; Springer Berlin Heidelberg, 2004; Vol. *234* pp 97−128.
(163) Halcrow, M. A. Structure:Function Relationships in Molecular Spin-Crossover Materials. In *Spin-Crossover Materials*; John Wiley and Sons Ltd: Oxford, UK, 2013; pp 147−169.
(164) Ericsson, M.-S.; Jagner, S.; Ljungström, E.; Tørneng, E.; Woldbæk, T.; Strand, T. G.; Sukhoverkhov, V. F. The Crystal Structure of Hexakis(Phenylisocyanide)Manganese(I) Tri-Iodide, $[Mn(CNC_6H_5)_6]I_3$. *Acta Chem. Scand.* **1980**, *34a*, 535−540.
(165) Cotton, F. A.; Zingales, F. The Donor-Acceptor Properties of Isonitriles as Estimated by Infrared Study. *J. Am. Chem. Soc.* **1961**, *83*, 351−355.
(166) Hahn, F. E. The Coordination Chemistry of Multidentate Isocyanide Ligands. *Angew. Chem., Int. Ed.* **1993**, *32*, 650−665.
(167) Margulieux, G. W.; Weidemann, N.; Lacy, D. C.; Moore, C. E.; Rheingold, A. L.; Figueroa, J. S. Isocyano Analogues of $[Co(CO)_4]^n$: A Tetraisocyanide of Cobalt Isolated in Three States of Charge. *J. Am. Chem. Soc.* **2010**, *132*, 5033−5035.
(168) Ditri, T. B.; Carpenter, A. E.; Ripatti, D. S.; Moore, C. E.; Rheingold, A. L.; Figueroa, J. S. Chloro- and Trifluoromethyl-Substituted Flanking-Ring *m*-Terphenyl Isocyanides: H_6-Arene Binding to Zero-Valent Molybdenum Centers and Comparison to Alkyl-Substituted Derivatives. *Inorg. Chem.* **2013**, *52*, 13216−13229.
(169) Ditri, T. B.; Moore, C. E.; Rheingold, A. L.; Figueroa, J. S. Oxidative Decarbonylation of *m*-Terphenyl Isocyanide Complexes of Molybdenum and Tungsten: Precursors to Low-Coordinate Isocyanide Complexes. *Inorg. Chem.* **2011**, *50*, 10448−10459.
(170) Carpenter, A. E.; Margulieux, G. W.; Millard, M. D.; Moore, C. E.; Weidemann, N.; Rheingold, A. L.; Figueroa, J. S. Zwitterionic Stabilization of a Reactive Cobalt Tris-Isocyanide Monoanion by Cation Coordination. *Angew. Chem., Int. Ed.* **2012**, *51*, 9412−9416.
(171) Claude, G.; Salsi, F.; Hagenbach, A.; Gembicky, M.; Neville, M.; Chan, C.; Figueroa, J. S.; Abram, U. Structural and Redox Variations in Technetium Complexes Supported by *m*-Terphenyl Isocyanides. *Organometallics* **2020**, *39*, 2287−2294.
(172) Pižl, M.; Hunter, B. M.; Sazanovich, I. V.; Towrie, M.; Gray, H. B.; Záliš, S.; Vlček, A. Excitation-Wavelength-Dependent Photophysics of d^8d^8 Di-Isocyanide Complexes. *Inorg. Chem.* **2022**, *61*, 2745−2759.
(173) Nielson, R. M.; Wherland, S. Reduction Potential and Bonding Trends in Manganese(I) and Manganese(II) Hexakis(Aryl and Alkyl Isocyanides). *Inorg. Chem.* **1985**, *24*, 1803−1808.

https://doi.org/10.1021/acs.inorgchem.2c01438
Inorg. Chem. 2022, 61, 10533−10547

(174) Sutton, G. D.; Olumba, M. E.; Nguyen, Y. H.; Teets, T. S. The Diverse Functions of Isocyanides in Phosphorescent Metal Complexes. *Dalton Trans.* **2021**, *50*, 17851−17863.
(175) Joshi, K. K.; Pauson, P. L.; Stubbs, W. H. Isocyanide Metal Complexes I. Reactions of Halocarbonyls with Phenylisocyanide. *J. Organomet. Chem.* **1963**, *1*, 51−57.
(176) Fantucci, P. C.; Valenti, V.; Cariati, F. Electronic Spectra of Some Isocyanide Complexes. *Inorg. Chim. Acta* **1971**, *5*, 425−428.
(177) Fantucci, P.; Naldini, L.; Cariati, F.; Valenti, V.; Bussetto, C.; Snam Progetti, L. S. R. The Electronic Structure of Isocyanide Ligands and the Spectroscopic Behaviour of Mn^{II} Octahedral Complexes. *J. Organomet. Chem.* **1974**, *64*, 109−124.
(178) Sarapu, A. C.; Fenske, R. F. Transition Metal-Isocyanide Bond. Approximate Molecular Orbital Study. *Inorg. Chem.* **1975**, *14*, 247−253.
(179) Verdonck, L.; Tulun, T.; van der Kelen, G. P. Far-I.R. and Raman Spectra of $(RNC)_6Mn^+$ Compounds (R = CH_3, C_6H_5, 4-Cl-C_6H_4). *Spectrochim. Acta, Part A* **1979**, *35*, 867−870.
(180) Cameron, C. J.; Walton, R. A.; Edwards, D. A. The Vibrational Spectra of the Homoleptic Isocyanide Complexes $[Re(CNR)_6]PF_6$, (R = Me, Ph, and 4-MeC_6H_4). *J. Organomet. Chem.* **1984**, *262*, 335−346.
(181) Wagner, N. L.; Wüest, A.; Christov, I. P.; Popmintchev, T.; Zhou, X.; Murnane, M. M.; Kapteyn, H. C. Monitoring Molecular Dynamics Using Coherent Electrons from High Harmonic Generation. *Proc. Natl. Acad. Sci. U.S.A.* **2006**, *103*, 13279−13285.
(182) Chapados, C.; Birnbaum, G. Infrared Absorption of SF_6 from 32 to 3000 cm^{-1} in the Gaseous and Liquid States. *J. Mol. Spectrosc.* **1988**, *132*, 323−351.
(183) Elgrishi, N.; Rountree, K. J.; McCarthy, B. D.; Rountree, E. S.; Eisenhart, T. T.; Dempsey, J. L. A Practical Beginner's Guide to Cyclic Voltammetry. *J. Chem. Educ.* **2018**, *95*, 197−206.
(184) Henke, W. C.; Otolski, C. J.; Moore, W. N. G.; Elles, C. G.; Blakemore, J. D. Ultrafast Spectroscopy of $[Mn(CO)_3]$ Complexes: Tuning the Kinetics of Light-Driven CO Release and Solvent Binding. *Inorg. Chem.* **2020**, *59*, 2178−2187.
(185) Kottelat, E.; Lucarini, F.; Crochet, A.; Ruggi, A.; Zobi, F. Correlation of MLCTs of Group 7 *fac*-$[M(CO)_3]^+$ Complexes (M = Mn, Re) with Bipyridine, Pyridinylpyrazine, Azopyridine, and Pyridin-2-ylmethanimine Type Ligands for Rational PhotoCORM Design. *Eur. J. Inorg. Chem.* **2019**, *2019*, 3758−3768.
(186) Ford, P. C. From Curiosity to Applications. A Personal Perspective on Inorganic Photochemistry. *Chem. Sci.* **2016**, *7*, 2964−2986.
(187) Krishnan, C. V.; Creutz, C.; Mahajan, D.; Schwarz, H. A.; Sutin, N. Homogeneous Catalysis of the Photoreduction of Water by Visible Light. 3. Mediation by Polypyridine Complexes of Ruthenium(II) and Cobalt(II). *Isr. J. Chem.* **1982**, *22*, 98−106.
(188) Vaidyalingam, A.; Dutta, P. K. Analysis of the Photodecomposition Products of $Ru(bpy)_3^{2+}$ in Various Buffers and upon Zeolite Encapsulation. *Anal. Chem.* **2000**, *72*, 5219−5224.
(189) Soupart, A.; Alary, F.; Heully, J. L.; Elliott, P. I. P.; Dixon, I. M. Recent Progress in Ligand Photorelease Reaction Mechanisms: Theoretical Insights Focusing on Ru(II) ^{3}MC States. *Coord. Chem. Rev.* **2020**, *408*, No. 213184.
(190) Herr, P.; Glaser, F.; Büldt, L. A.; Larsen, C. B.; Wenger, O. S. Long-Lived, Strongly Emissive, and Highly Reducing Excited States in Mo(0) Complexes with Chelating Isocyanides. *J. Am. Chem. Soc.* **2019**, *141*, 14394−14402.
(191) Büldt, L. A.; Guo, X.; Prescimone, A.; Wenger, O. S. A Molybdenum(0) Isocyanide Analogue of $Ru(2,2'\text{-Bipyridine})_3^{2+}$: A Strong Reductant for Photoredox Catalysis. *Angew. Chem., Int. Ed.* **2016**, *55*, 11247−11250.

https://doi.org/10.1021/acs.inorgchem.2c01438
Inorg. Chem. 2022, 61, 10533−10547